

Review

Stimuli-activatable nanomedicine meets cancer theranostics

Haonan Li^{1,*}, Yue Feng^{1,*}, Qiang Luo^{1,*}, Zhiqian Li¹, Xue Li¹, Huatian Gan¹, Zhongwei Gu¹, Qiyong Gong^{1,2,3}, Kui Luo^{1,2,✉}

1. Department of Radiology, and Department of Geriatrics, Laboratory of Heart Valve Disease, Huaxi MR Research Center (HMRR), Laboratory of Stem Cell Biology, National Clinical Research Center for Geriatrics, Frontiers Science Center for Disease-Related Molecular Network, State Key Laboratory of Biotherapy, West China Hospital, Sichuan University, No. 37 Guoxue Alley, Chengdu 610041, China.
2. Functional and Molecular Imaging Key Laboratory of Sichuan Province and Research Unit of Psychoradiology, Chinese Academy of Medical Sciences, Chengdu 610041, China
3. Department of Radiology, West China Xiamen Hospital of Sichuan University, 699 Jinyuan Xi Road, Jimei District, 361021 Xiamen, Fujian, China.

*Those authors contributed equally to this work.

✉ Corresponding author: E-mail: luokui@scu.edu.cn.

© The author(s). This is an open access article distributed under the terms of the Creative Commons Attribution License (<https://creativecommons.org/licenses/by/4.0/>). See <http://ivyspring.com/terms> for full terms and conditions.

Received: 2023.07.06; Accepted: 2023.09.05; Published: 2023.10.02

Abstract

Stimuli-activatable strategies prevail in the design of nanomedicine for cancer theranostics. Upon exposure to endogenous/exogenous stimuli, the stimuli-activatable nanomedicine could be self-assembled, disassembled, or functionally activated to improve its biosafety and diagnostic/therapeutic potency. A myriad of tumor-specific features, including a low pH, a high redox level, and overexpressed enzymes, along with exogenous physical stimulation sources (light, ultrasound, magnet, and radiation) have been considered for the design of stimuli-activatable nano-medicinal products. Recently, novel stimuli sources have been explored and elegant designs emerged for stimuli-activatable nanomedicine. In addition, multi-functional theranostic nanomedicine has been employed for imaging-guided or image-assisted antitumor therapy. In this review, we rationalize the development of theranostic nanomedicine for clinical pressing needs. Stimuli-activatable self-assembly, disassembly or functional activation approaches for developing theranostic nanomedicine to realize a better diagnostic/therapeutic efficacy are elaborated and state-of-the-art advances in their structural designs are detailed. A reflection, clinical status, and future perspectives in the stimuli-activatable nanomedicine are provided.

Keywords: exogenous stimuli; Endogenous stimuli; stimuli activation; nanomedicine; cancer theranostics

1. Introduction

Cancer theranostics (e.g., chemotheranostics, radiotheranostics, immunotheranostics, and phototheranostics) have shown tremendous promise in cancer management [1]. A nanoscale size or a nanostructure endows these theranostic products with a high specific surface area, tunable physicochemical properties, flexible imaging/therapeutic functions, and improved biocompatibility. Theranostic nanomedicine has been designed and constructed for better cancer management than current theranostic products for diagnosis and therapy [2]. For example, disease-specific biomarker-targeting ligands have been incorporated into nanostructures

with imaging properties for early cancer detection and accurate profiling of tumors. Furthermore, visualization of chemotherapeutic drugs, photo-/radio-/sono-sensitizers, tumor vaccines, immune regulators, and immune cells via nanostructures with imaging properties could revolutionize the entire cancer management procedure [3, 4]. Additionally, versatile modification and/or manipulation of nanostructures create greater room for cancer theranostics, for example, real-time single/dual/multiplex imaging modality-guided or imaging-assisted cancer treatment [5, 6].

Theranostic nanomedicine can reach tumor sites

with a high cargo load through the enhanced permeability and retention (EPR) effect or the modification with active targeting moieties [7], while controlled or smart release of the cargo in the nanomedicine can avoid systemic adverse effects and circumvent a compromised potency due to burst or pre-leaked release. In this context, stimuli-activatable tactics in designing and constructing theranostic nanomedicine have been proposed. Specifically, unique characteristics of the tumor microenvironment (TME), including a low pH, a high redox level, hypoxia, and overexpressed specific enzymes, have been explored for stimuli-activatable theranostics to achieve tumor-specific management [8]. Moreover, mechanical forces exerted from light, radiation, magnetic field, and ultrasound have been employed for vascular transportation, activation, or degradation of theranostic nanomedicine to realize potent, targeted therapy with remarkably reduced adverse effects. These bioactivatable nanomedicinal products are often designed with an activatable structure before reaching tumor sites, while their structures are disassembled, re-assembled, or activated in response to the TME characteristics or external physical forces [9], reaching a balance between their on-target efficacies and off-target toxicity for better cancer management.

After these exogenous/endogenous stimuli alter the structure of the nanomedicine products, imaging agents/drugs could be released from the nanostructures for directly exerting imaging/therapeutic effects or they are aggregated for enhancing their imaging and/or therapeutic potencies. In terms of imaging, specific endogenous stimuli or exogenous physical forces could help expose, activate, or aggregate the imaging moiety in the nanomedicine, thus boosting imaging signal intensity. Novel strategies for stimuli-triggered signal-switch in the nanomedicine have emerged, for instance, manipulating the relative distance between a signal emitter/enhancer and a quencher in a hollow nanostructure. The nanostructure could be loaded with imaging, therapeutic, or theranostic agents and it is also equipped with modifiable gatekeepers or degradable compartments that are sensitive to a specific stimulus. In response to the stimulus, the nanostructure or the linker could be deformed/degraded to increase the distance between the pro-quenched or protective agents and their signal emitters/enhancers or bioactive agents, thus triggering a “switch-on” for its activatable or switchable imaging function [10]. Furthermore, since some of inorganic nanoagents have imaging/therapeutic function, the detachment of their surface coating may lead to aggregation of inorganic

nanoagents for enhanced imaging (e.g., computed tomography (CT), T2-weighted image (T2WI) of magnetic resonance imaging (MRI), photoacoustic imaging (PAI), and aggregation-induced emission (AIE)) and/or antitumor therapeutic efficacies (e.g., photothermal therapy (PTT) and radiotherapy (RT)). In addition, to design stimuli-activatable theranostic nanostructures, theranostic nanoagents (e.g., MnO₂ and polydopamine) with inherent stimuli-responsive imaging/therapy properties could be utilized to boost the therapeutic/imaging efficacy. A few stimuli-activatable theranostic strategies, including simultaneous/sequential/cascade activation, integration of dual/multiplex endogenous stimuli, and combination of endogenous stimuli with exogenous ones have gained popularity.

A few stimuli-activatable nanostructures have entered clinical trials or used in clinical practice, such as thermo-sensitive DOX-loading liposomes (ThermoDox®) and ONM-100 (a pH-sensitive fluorescent polymeric nanoparticle conjugated with indocyanine green). They have exhibited improved bioavailability and/or an encouraging diagnostic efficiency [11]. These inspiring results indicate that the application of stimuli-activatable tactics in developing theranostic nanomedicine could hold great potential for treating advanced cancer. In this review, we reveal the indispensable role of theranostics in the long-lasting clinical need for cancer management. Stimuli-activatable strategies for designing nanomedicine for theranostics are elaborated, with emphasis on endogenous/exogenous stimuli and their corresponding activatable ligands/structures, as well as the activatable mechanisms, which have not been systematically reviewed before. Additionally, state-of-the-art application of activatable cancer theranostic nanomedicine is surveyed. Finally, the current clinical status, along with a reflection and future perspectives of activatable theranostic nanomedicine are presented (Figure 1).

2. Stimuli-activatable strategies for nanomedicine-assisted cancer theranostics

2.1. Nanomedicine embraces cancer theranostics

With tunable imaging properties and improved pharmacokinetics, nanomedicine emerges as an important addition to the existing imaging and therapeutic modalities [12]. The nanomedicine for cancer theranostics works in various regimes based on therapeutic modalities, including chemotheranostics, radiotheranostics, immunotheranostics, phototheranostics, sonotheranostics, and image-guided therapy

(Figure 2).

Generally, a variety of theranostic nanoplat-forms, including supramolecular architectures, polymeric architectures, inorganic architectures, and hybrid architectures have emerged to hold one single agent or both imaging and therapeutic agents for synergistic theranostics [13, 14]. The intratumoral or

intranasal distribution of visible nanoparticles have the potential of quantitatively assessing their tumor accumulation/tumor penetration/cellular internalization/lymph node infiltration, spatiotemporally monitoring drug release, accurately predicting therapeutic response, and enabling effective image-guided therapy.

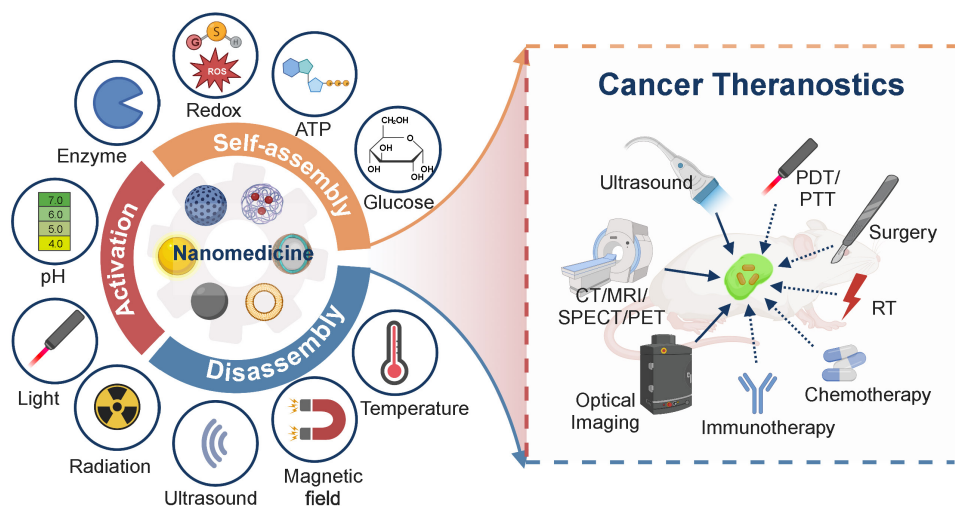


Figure 1. Scheme for stimuli-activatable nanomedicine-assisted cancer theranostics. Activatable cancer nanomedicine is designed to be sensitive to endogenous (a low pH, over-expressed enzymes, an elevated concentration of active small molecules including redox agents, ATP, and glucose) and/or exogenous stimuli (light, radiation, ultrasound, magnetic field, and temperature), thus improving the efficacy of cancer theranostics, an integration platform of imaging modalities indicated by solid arrows (ultrasound, CT, MRI, PET, SPECT, and optical imaging) and therapeutic approaches indicated by dashed arrows (PDT/PTT, surgery, RT, chemotherapy, and immunotherapy). PET: positron emission tomography; SPECT: single photon emission computed tomography; PDT: photodynamic therapy; RT: radiotherapy.

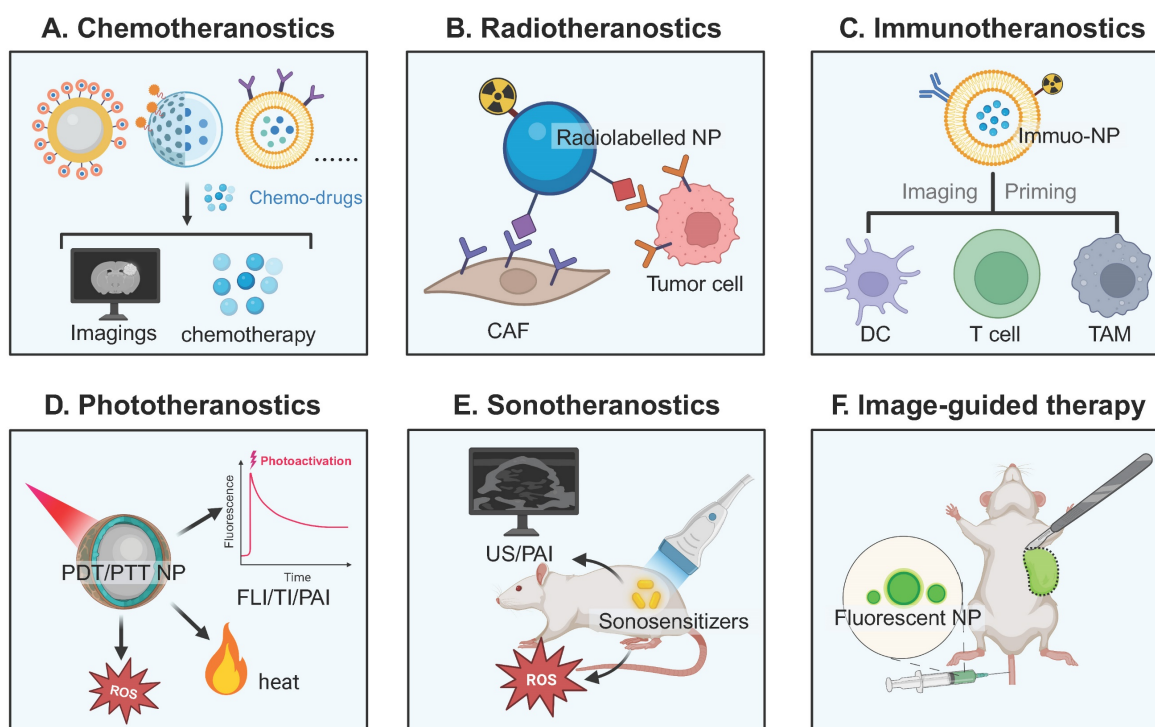


Figure 2. Schematic of nanomedicine in different theranostic regimes based on treatment approaches. A) Chemotheranostics: various nanoformulations deliver chemotherapeutic molecules (some of them are optically visible) and imaging agents. B) Radiotheranostics: diagnostic/therapeutic radionuclides-labeled nanoparticles target tumor cells or CAFs. C) Immunotheranostics: nanomedicine is designed to image and prime immune cells, including DCs, T cells, and TAMs. D) Phototheranostics: light induces response from nanomedicine to generate imaging signals in FLI/TI/PAI or exert therapeutic effects of therapeutic agents (ROS and heat) in fluorescence imaging-guided PDT and/or PAI-guided PTT. E) Sonotheranostics: ultrasound at a low intensity triggers sonosensitizers to improve ultrasound imaging contrast and/or generate toxic ROS in tumor cells. F) Image-guided therapy including image-guided surgery and image-guided cell therapies: pre-injection of fluorescent NPs or other optically visible probes aids in delineating tumor margins or sentinel lymph nodes for surgery. NP: nanoparticle; CAF: cancer-associated fibroblast; DC: dendritic cell; TAM: tumor-associated macrophage; FLI: fluorescence imaging; TI: thermal imaging; ROS: reactive oxygen species; US: ultrasound; PAI: photoacoustic imaging.

2.2. Stimuli-activatable strategies: why adopt them?

There lie several obstacles in the application of nanomedicine-assisted cancer theranostics, including high background noises for imaging, long-term body retention, and unspecific/uncontrolled drug release [15]. To overcome these obstacles, a few stimuli-activatable strategies have been proposed for developing cancer theranostic nanomedicine in response to various unique TME characteristics and exogenous physical stimuli. Response of the nanomedicine to these stimuli results in stability/shape/charge/size alterations and prompts self-assembly, disassembly, or activatable function transformation, eventually contributing to an improved theranostic performance. Specifically, these stimuli-activatable strategies have the following advantages.

i. Enhanced tumoral biodistribution, penetration, and retention of activatable theranostic nanomedicine. Endogenous stimuli can break the linker of the nanomedicine to detach protective coatings such as PEG or DNA threads [16], resulting in a decrease in the nanoparticle size, in-situ formation of a nanoassembly, negative-to-positive charge reversal, or release of active agents. Meanwhile, exogenous stimuli can convert an inactive status of theranostic agents (e.g., PDT/PTT nanoagents and sonosensitizers) into active one. Besides, they can remotely alter the TME (e.g., improving vascular penetration) and the *in vivo* behavior of the nanocarrier, leading to improved tumor accumulation and controllable release kinetics [17]. Through exerting endogenous or exogenous stimuli on the nanomedicine, homogenous intratumoral distribution, enhanced tumoral penetration, and prolonged tumoral retention of imaging/therapeutic agents can be achieved via transformation of the nanostructure of the nanomedicine including self-assembly, disassembly, or activation [18, 19]. For example, stimuli-triggered size reduction of nanomedicine with 100-200 nm (an optimal size for the EPR effect) to 7-50 nm facilitates deep penetration in the solid tumor tissue, while a reduced size < 7 nm enables internalization nuclear targeting [20].

ii. Activatable imaging. The stimuli-activated strategy for designing the nanomedicine for imaging, especially Near-Infrared-II fluorescence imaging and photoacoustic imaging, could remarkably improve the signal-to-noise ratio (SNR) with reduced background noises and enable imaging at a deep distance compared with conventional probes with an “always-on” mode [21]. Notably, the distance between a fluorescent emitter and a quencher or a

T1/T2 MRI probe can be manipulated for an off-to-on switch to improve the imaging performance [22]. For example, a low pH, a high ROS level, a high glutathione (GSH) concentration, or an electric field could help detach surface coatings and extend the distance between Fe₃O₄ and Gd/Mn, leading to a switch-on of the T1 signal [23-25]. Ratiometric optical imaging of different cellular locations after single or dual light excitation can also be realized by utilizing the distinctive distribution of certain stimuli [26]. Meanwhile, stimuli-induced aggregation of imaging nanoagents is conducive to contrast intensification in CT, PAI, and PET/SPECT. In addition, optical nanoprobe, PAI nanoagents, quenched contrast agents, afterglow, and luminescence nanomedicine can be activated by exogenous stimuli (light and X-ray). Activatable imaging of elevated endogenous stimuli generated by therapy, such as ROS and caspase-3, can be employed for therapeutic response assessment via using corresponding stimuli-activatable imaging nanoagent [23, 27].

iii. Biodegradability. After the initial imaging evaluation or therapy, these stimuli-activatable nanostructures have released their cargos, and their nanocarriers are ready for clearance from the body [28, 29], particularly the inorganic one, since long-term retention of these nanocarriers in the human body could result in undesirable toxicity. For instance, stimuli-activated size shrinkage of the nanostructures into renal-clearable nanoassemblies (size < 5.5 nm) aids in their fast elimination [30]. Moreover, the addition of stimuli-sensitive linkers to the polymer backbone facilitates their degradation into small fragments (Mw < 45 kDa) for renal excretion after cleavage of these linkers.

iv. Reduced toxicity. Surface shielding of the nanomedicine via stimuli-activatable ligands (e.g., protease-cleavage substrates) is a masking method to alleviate severe side effects of the imaging/therapeutic agents in the nanomedicine in adjacent normal tissues and enable on-demand release of them in tumor tissues.

Endogenous stimuli are often considered for stimuli-activatable nanomedicine prodrugs in current pre-clinical practices, while exogenous stimuli are explored for synergistically combined treatment. Response to either endogenous or exogenous stimuli results in in-situ self-assembly, disassembly, and functional activation in the stimuli-activatable nanomedicine; self-assembly and disassembly represent two typical types of structural transformation during the procedure of stimuli-activation, and activation refers to different activation modes of specific function of the nanomedicine (Figure 3).

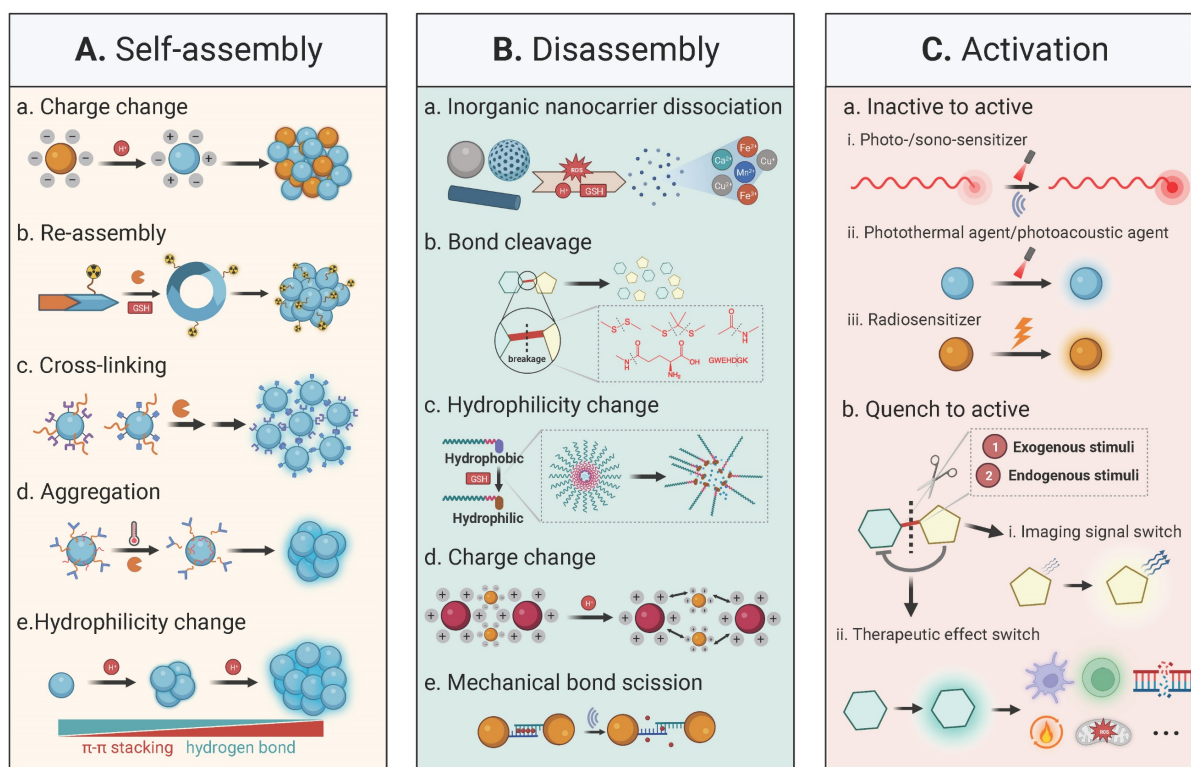


Figure 3. Illustration of self-assembly, disassembly, and activation of nanomedicine. A) Interactions between molecular complexes or nanoparticles, including hydrophobic interaction, hydrogen bonding, electrostatic interaction, host-guest interaction, and dipole-dipole interaction, as well as magnetic or electric forces contribute to stimuli-induced self-assembly. B) Disassembly is realized through morphological/structural transformation/dissociation, bond cleavage, removal of hydrophilic units, charge change, mechanical bond scission, deprotection, cascade reaction, and fragmentation to monomers or oligomers. C) Introducing an activatable energy source or removing a quenched chemical moiety induces the activation of functional moieties in the nanomedicine.

Overall, the ultimate goal of cancer nanomedicine is to achieve the maximum therapeutic benefit with tolerant toxicity, thus stimuli-activatable strategies are the most preferable option to fabricate the nanomedicine.

2.3. Endogenous or exogenous stimuli and their corresponding activatable ligands

With joint efforts by cancer biologists, biomedical scientists, chemists, and biomaterial scientists, unique features of the TME have been unveiled and chemical ligands or peptides that are sensitive to these features have been thereafter developed. A brief introduction of various identified endogenous/exogenous stimuli is presented below.

Low pH. Tumor cells are conventionally featured with a pH gradient inside cells and between cells: intracellular ($\text{pH}_i \geq 7.2$) except for early endosomes (pH 6.3), late endosomes (pH 5.5), and lysosomes (pH 4.7) and extracellular ($\text{pH}_e = 6.7\text{--}7.1$) [31]. Cancer nanomedicine often experiences the pH gradient during the transportation process from a physiological pH of 7.4, an extracellular pH of 6.7–7.1, and an acidic endosomal/lysosomal pH of 4.7–6.3.

ROS. Reactive oxygen species (ROS) are mainly composed of superoxide ($\text{O}_2^{\cdot-}$), hydroxyl radical ($\cdot\text{OH}$), nitric oxide ($\text{NO}\cdot$), hydrogen peroxide (H_2O_2),

singlet oxygen ($^1\text{O}_2$), and organic hydroperoxides (ROOH) [32, 33]. The main sources for endogenous ROS are mitochondrial metabolism, peroxisomes, and the activity of the transmembrane NADPH oxidases family [34, 35]. In addition, exogenous mechanical forces (e.g., light and radiation) can disrupt the redox imbalance, leading to an elevated ROS level.

GSH. Glutathione (GSH), a low-molecular-weight peptide, consists of glutamate, cysteine, and glycine. There is a three-order-of-magnitude difference in the GSH concentration in tumor cells, *i.e.*, 2–10 μM in extracellular spaces and 1–10 mM in intratumor cells [36].

Over-expressed enzymes. Tumor-associated enzymes are over-expressed in different subcellular localizations. These over-expressed enzymes with their locations are detailed: extracellular environment (matrix metalloproteinase) [37]; cell membrane (alkaline phosphatase, aminopeptidase N, and γ -glutamyltranspeptidase) [38]; cytosol (transglutaminase, autophagy-related 4B cysteine peptidase, nitroreductase, and caspase-3/7) [39]; lysosome (cathepsin B, β -galactosidase, and β -glucuronidase) [40, 41]; endoplasmic reticulum (carboxylesterase and protein tyrosine phosphatase 1B) [42]; Golgi (furin) [43]; mitochondrion (enterokinase) [44]; and nuclear (endonuclease histone deacetylases) [45].

Elevated ATP levels. The adenosine-5'-triphosphate (ATP) level in an intracellular environment (1-10 mM) of tumor cells is much higher than that in an extracellular environment (<0.4 mM) [46].

Elevated glucose metabolism. Accelerated aerobic glycolysis or a rapid cellular glucose metabolic rate to support tumor cell proliferation, which is often accompanied with a high glucose flux, is recognized as a hallmark of cancer [47]. Glucose oxidase (GOx), an enzyme which is sensitive to intracellular glucose, has been widely exploited to prepare glucose-responsive nanomedicine for cancer theranostics [48].

Hypoxia. Tumor hypoxia originates from vigorous tumor metabolic activities and a deficiency in the O₂ transfer from vascularity at a long distance away. Euhypoxia (a physicochemical gradient of oxygen), nitroreductase, and their associated features (adenosine, acidosis, and nutrient deficiencies) are quite distinctive in the TME [49].

Other endogenous stimuli. Other abundantly-expressed agents in tumor areas, such as H₂S [50], nitric oxide (NO) [51], metal ions (Ca²⁺) [52], and TK1 mRNA [53], have also been exploited as endogenous stimuli for activatable nanomedicine.

Light. Light is used as an activation energy source for nanomedicine-assisted multiplexed therapy (PDT, PTT, and surgery) and imaging (PAL, fluorescence imaging, and thermal imaging) modalities. Without exposure to light, the activatable nanomedicine remains dormant and inefficacious. Upon exposure to light, these responsive agents are activated to realize generation of toxic agents (ROS and heat), stimuli-triggered drug release, and a turn-on of imaging [54, 55].

Ultrasound. Ultrasound, a widely used imaging tool, can directly trigger the tumor-killing effect via ultrasonic cavitation and a mechanical and thermal effect in the form of high-intensity focused ultrasound (HIFU), as well as indirectly induce the opening of the blood-brain barrier, destruct imaging-guided gas-filled microbubbles to exert physical stress to cancer cells, and generate sonoluminescence for cancer detection [56].

Radiation. Radiation (e.g., X-ray, γ -ray, other charged particles) with an intensive energy can directly induce the degradation of prodrugs and inorganic nanostructures, such as sulfonyl azide- and phenyl azide-caged prodrugs of pazopanib and doxorubicin [57] and a hierarchical metallic supra-nanostructure with thin Au branches connected with Ag nano-linkers [58]. Furthermore, radiation can indirectly generate ROS or hydrated electrons in tumors, resulting in the breakage of ROS-activatable linkers or quaternary ammonium masking groups

[59]. Notably, the unlimited penetration capacity of radiation allows for enhancing photodynamic therapy, fluorescence imaging, and X-ray-excited persistent luminescence for deeply-seated tumors [60].

Magnetic field. Magnetic nanoparticles or nanorobots, particularly, the Fe-based one, can be driven by an external magnetic field (e.g., an alternating magnetic field (AMF)) to achieve their localized accumulation and/or generate magnetic hyperthermia. In this procedure, magnetic particle-assisted imaging or T2WI MRI as well as the magnetothermal effect-triggered cargo release from the nanomedicine can be realized [61, 62].

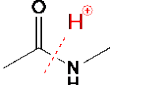
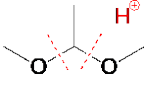
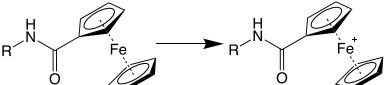
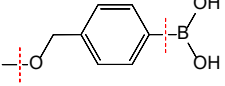
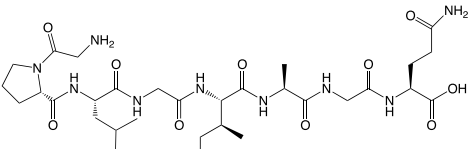
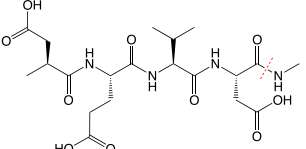
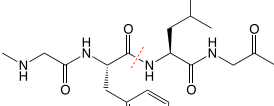
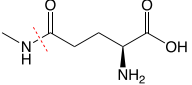
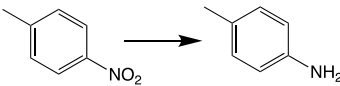
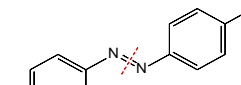
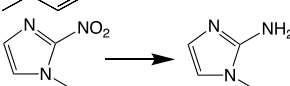
Thermal. The localized thermal effect can be elicited by focused ultrasound, magnetic hyperthermia, light-activated photothermal nanoagents, microwave thermal therapy, and microwave dynamic therapy [63]. The rise in the local temperature can help generate thermal images, boost the responsiveness of temperature-sensitive linkers, activate thermally activated fluorescent (TADF) nanoagents, and improve the activity of therapeutic enzymes [64].

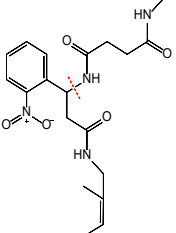
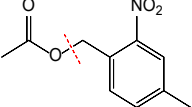
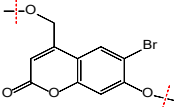
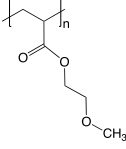
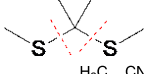
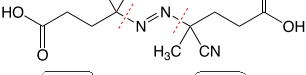
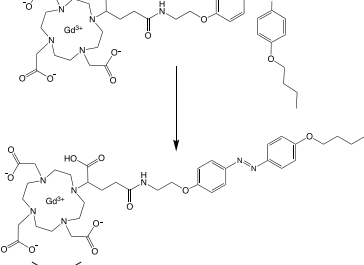
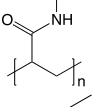
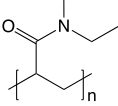
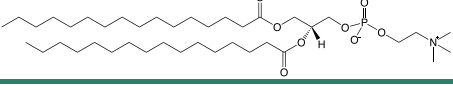
The endogenous/exogenous stimuli-activatable linkers and their activatable reaction mechanisms have been well summarized elsewhere [9, 65]. Herein, we list representative linkers and their chemical structures (Table 1). To note, biodegradable inorganic nanostructures, such as mesoporous organosilica and metal oxide (e.g., CaCO₃ and MnO₂), are a major type of stimuli-activatable nanomedicine and an important supplement to this Table [66, 67].

Efforts have been devoted to exploring rational design and elegant manipulation of activatable linkers in the nanomedicine, as well as developing efficient alternative ones. An ultra-pH-sensitive nanoparticle library with precisely tuned pH transitions (pH_t = 4.0-7.4) was prepared by co-polymerization of a tertiary amine-containing monomer with a group of non-ionizable monomers, and the hydrophobicity of the non-ionizable monomer played an important role in the pH tunability [94]. Moreover, chemical structures that are sensitive to dual or multiple stimuli have attracted great attention. For example, poly(*N,N*-dimethylaminoethyl methacrylate) (PDMAEMA) can be both pH-activatable and thermo-activatable [95]. Several redox-activatable bonds with dual ROS/GSH-responsivity were designed on basis of sulfur-tellurium-sulfur and sulfur-selenium-sulfur hybrid chalcogen bonds [96]. A generalized polymeric delivery system by integrating various stimuli-activatable bonds via logic gates has been proposed for controlled sequential release of drug cargos [97]. Besides, the release/activation modes, such as immediately

activated, sustainedly activated, progressively activated, and pulsatively activated, could be explored for optimized design of various nanostructures for the activatable nanomedicine.

Table 1. Selected activatable ligands toward endogenous/exogenous stimuli

| Stimulus | Activatable ligand and descriptions | Chemical structure or transition process | Ref |
|----------|--|--|------|
| pH | Amide bond or bridge: cleavage |  | [68] |
| | Acetal bond: cleavage |  | [69] |
| | Poly(β -amino esters): amine protonation |  | [70] |
| GSH | Disulfide bond: cleavage |  | [71] |
| | Diselenide bond: cleavage |  | [72] |
| ROS | $^1\text{O}_2$ -activatable thioketals: cleavage |  | [73] |
| | H_2O_2 -activatable ferrocene: hydrophobic to hydrophilic transformation |  | [74] |
| Enzyme | H_2O_2 -sensitive phenylboronic acid |  | [75] |
| | MMP2-cleavable peptide PLGIAG |  | [76] |
| | Caspase 3/7-cleavage DEVD peptide (Asp-Glu-Val-Asp) |  | [27] |
| | Cathepsin B-cleavage GFLG tetrapeptide (Gly-Phe-Leu-Gly) |  | [77] |
| Hypoxia | GGT-cleavage γ -glutamyl moieties |  | [78] |
| | A cleavable p-nitrobenzyl group by nitroreductase |  | [79] |
| | Azobenzenes (AZO): reduction |  | [80] |
| | 2-nitroimidazole: hydrophobic to hydrophilic transformation |  | [81] |

| Stimulus | Activatable ligand and descriptions | Chemical structure or transition process | Ref |
|--------------------|--|--|------|
| Light | Photocleavable linker (PCL) |  | [82] |
| | Photolysis of <i>O</i> -nitrobenzyl ester |  | [83] |
| | Light-cleavable coumarin ester |  | [84] |
| US | pMEMA: poly(methoxyethyl methacrylate) |  | [85] |
| | Indirect breakage of thioketal bonds with the aid of a sonosensitizer |  | [86] |
| | Cleavage of ACVA C-N bonds |  | [87] |
| Ionizing radiation | Reduction of <i>N</i> -oxide |  | [88] |
| | Diselenid bond: cleavage |  | [89] |
| | Geometrical structure transformation: <i>cis</i> -GdAzo to <i>trans</i> -GdAzo |  | [90] |
| Thermal | Poly(<i>N</i> -isopropylacrylamide) (PNIPAAm) |  | [91] |
| | Poly[<i>(N,N</i> -diethyl)acrylamide] (pDEA) |  | [92] |
| | Dipalmitoyl phosphatidylcholine (DPPC): gel to liquid-crystalline phase transition |  | [93] |

MMP2: matrix metalloproteinase 2; GGT: gamma-glutamyl transpeptidase; US: ultrasound; ACVA: 4,4'-Azobis(4-cyanovaleric acid).

Taken together, stimuli-enabled nanostructural transformation through stimuli-activatable linkers in the nanomedicine has been reported to improve the biodistribution of a variety of drugs, such as chemotherapeutic agents, immuno-cytokines, and PROteolysis Targeting Chimeras. Concerns over the sensitivity of activatable bonds to other stimuli have

been raised when the nanomedicine is prepared, thus novel synthesis methods, such as supercritical fluid-assisted fabrication, have emerged [98]. Activation/cleavage of endogenous stimuli-activatable linkers/chemical groups often consume these endogenous stimuli (ROS, GSH, and protons); in this procedure, the adverse effects induced by these

stimuli, such as promoting tumor progression and retaining an immunosuppressive TME, may be alleviated. However, this activation process does not consume enzymes. It may be hypothesized that the inactivation of an enzyme through enzyme-responsive linkers could help delay tumor progression or achieve a better prognosis after the breakage of the enzyme-activatable linkers in the nanomedicine.

3. State-of-the-art advances in stimuli-activatable nanomedicine for cancer theranostics

3.1. Cancer theranostics and theranostic nanoagents

In the current clinical setting, cancer theranostics refer to imaging-guided therapy and radiotheranostics using diagnostic/therapeutic radionuclides pairs. The former is the therapeutic intervention with the guidance of real-time imaging, such as ultrasound-guided punctation and resection, tumor removal based on stained fluorescent images, CT/MRI-guided delineation of the tumor location for precise radiotherapy, and gastroscopy or proctoscopy-guided surgery. With the application of nanotechnology in cancer theranostics, theranostic nanoagents by incorporating an agent with simultaneous imaging and therapy properties or multiple diagnostic/therapeutic agents into one single nanocarrier [99] have been developed for improved imaging-guided therapy, quantitative

control of the released drugs, and extended theranostic regimes (Table 2).

Table 2. Selected examples of theranostic nanoagents

| Nanoagents | Imaging methods | Therapeutic effects | Ref |
|---------------------------------------|---------------------------|---|-------|
| MnO ₂ NPs | MRI | Hypoxia relief; immunomodulation; Fenton reaction | [67] |
| Gd-based NPs | MRI | Radio-sensitization; Gd-NCT | [100] |
| AuNPs | PAI; CT; SERS | PTT; radiotherapy | [101] |
| Iron oxide NPs | MRI; MPI | Ferropitosis; chemodynamic therapy; magnetic hyperthermia | [102] |
| Other heavy metal oxide-based NPs | CT | PTT; radiotherapy | [103] |
| Ag ₂ S QDs | NIRF | PTT | [104] |
| Polydopamine | Thermal image; PAI | PTT | [105] |
| AI-Egen | Photoluminescence imaging | PDT | [106] |
| Theranostic radio-isotopes-labeled NP | SPECT or PET | Radiotherapy | [107] |

NPs: nanoparticles; Gd-NCT: gadolinium-neutron capture therapy; SERS: surface-enhanced Raman scattering; MPI: magnetic particle imaging; QDs: quantum dots; NIRF: near-infrared fluorescence; AI-Egen: aggregation-induced emission luminogens; Theranostic radionuclides: ⁴⁷Sc, ⁶⁴Cu, ⁶⁷Cu, ⁶⁷Ga, ⁷⁷As, ¹¹¹In, ¹²⁵I, ¹²⁵Sn.

3.2. Stimuli-activatable nanomedicine in theranostic application

In the context of stimuli-activatable cancer theranostics, endogenous/exogenous stimuli have been explored for developing stimuli-responsive nanomedicine to improve its therapeutic outcome accompanied with a bio-tolerable profile (Table 3).

Table 3. Representative examples of stimuli-activatable theranostic nanomedicine

| Stimuli | Activatable theranostic nanomedicine | Imaging approaches | Therapeutic methods | Tumor models | Ref |
|---------------------------|---|----------------------------|---|---------------------------------------|-------|
| pH | PPD@HPAP-CPDs/Rapa | FLI | Immunotherapy, chemotherapy | 4T1 (breast cancer) | [108] |
| | AuNNR-DCNP Ve | NIRF, PAI | RT, chemotherapy | MCF-7 (breast cancer) | [109] |
| | Au/BP@MS | MRI | SDT | MCF-7 (breast cancer) | [110] |
| Redox | P-DOA NPs | PAI | SDT | B16F10 (melanoma) | [111] |
| | MMV-Au-CDs-DOX | FLI | Chemotherapy, CDT | 4T1 (breast cancer) | [112] |
| | FDINs | PAI, FLI | PTT, chemotherapy | 4T1 (breast cancer) | [113] |
| Enzyme | Fe- ⁴ HA | PAI | PTT, ferroptosis | 4T1 (breast cancer) | [114] |
| | NRh-G-NPs | NIRF | PTT | U87MG (glioma) | [115] |
| | DQP/DMe NPs | FLI | Chemotherapy | A549 (lung cancer) | [116] |
| Other endogenous stimulus | AgNPs@GQDs-Gox | Fluorometry, FLI | Staving-like/metal ion/TA-induced apoptosis therapy | K299 (anaplastic large cell lymphoma) | [117] |
| | AzoCyS-N NPs | NIRF, PAI | PDT, PTT | HeLa (cervical cancer) | [118] |
| | GNPs@MRM/HAL | NIRF, PTI | PDT | 4T1 (breast cancer) | [119] |
| Light | LPAR-siRNA | TI, PAI, CT | Gene therapy, PTT | Panc-1 (pancreatic cancer) | [120] |
| | BLIPO-I/D | NIRF | Chemotherapy, PDT, PTT | SW1990 (pancreatic cancer) | [121] |
| | AIBME@IR780-APM NPs | NIRF, MRI | PDT, TDT | 4T1 (breast cancer) | [122] |
| Other exogenous stimuli | SCAN | Sonoafterglow luminescence | Immunotherapy, SDT | 4T1 (breast cancer) | [123] |
| | PTX-NFGs | MRI | MF-triggered chemotherapy | LCC-6-WT (breast cancer) | [124] |
| | ⁸⁹ Zr-TiO ₂ -MnO ₂ | PET, CLI | CRIC | CT26 (colorectal cancer) | [125] |

FLI: fluorescence imaging; SDT: sonodynamic therapy; CDT: chemodynamic therapy; TDT: thermodynamic therapy; TI: thermal imaging; CLI: Cherenkov luminescence imaging; CRIC: Cherenkov radiation-induced cancer therapy; MF: magnetic field.

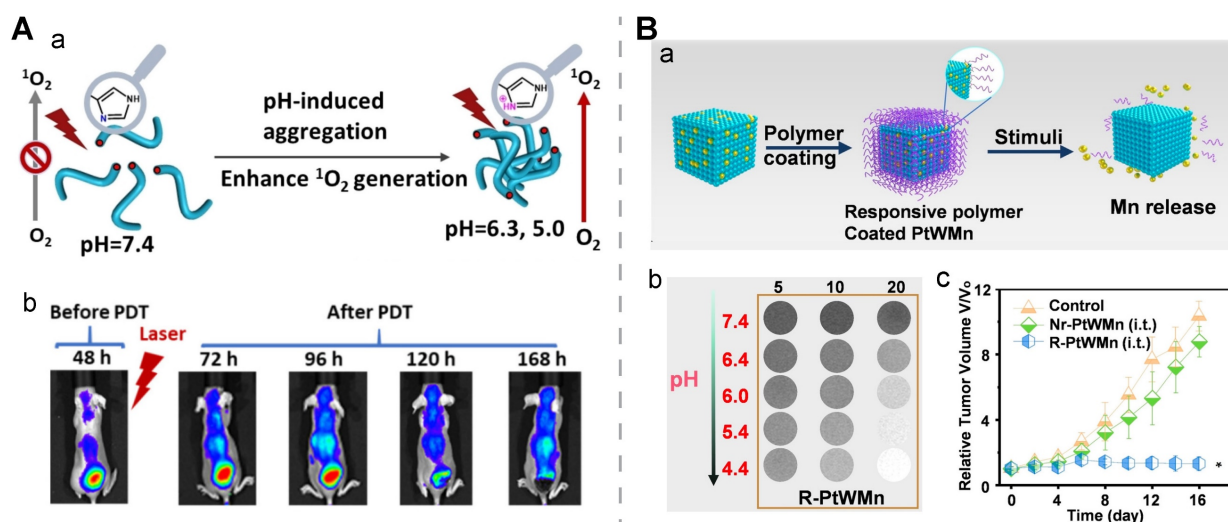


Figure 4. pH-activatable cancer theranostics. A) pH-induced aggregation of a porphyrin-peptide-based nanofiber via protonation for PDT and fluorescent imaging-aided prognosis. a) Schematic illustration. b) Fluorescence images of the mice at various time points post-injection. Reproduced with permission [132]. Copyright 2022 the Authors, published by Wiley-VCH. B) An activatable polymer-coated ternary alloy for MRI and ferroptosis therapy. a) Schematic design to illustrate that the detachment of activatable polymer coatings could promote release of metal ions in the core of the nanomedicine. b) T1-weighted MR images of R-PtWMn with different concentrations at different pH values. c) Tumor growth curves after the treatment with the polymer-coated alloy and controls. Reproduced with permission [133]. Copyright 2022, Wiley-VCH.

3.2.1. pH-activatable theranostic nanomedicine

Tumor acidosis with a low pH has been widely used as an endogenous trigger to break pH-cleavable bonds and pH-sensitive biodegradable materials for activating pro-theranostic agents. Specifically, coordination bonds that are cleaved by protonation include carboxyl, imidazolyl, amino, amide, pyridine, phenolic hydroxyl, daunosamie, vinyl-ether, and vinyl-amino [126, 127]. And the general pH-sensitive nanocarriers can be divided into three main types: inorganic (e.g., calcium phosphate, MnO_2 , CaCO_3), organic (e.g., polydopamine and polyaniline), and hybrid (e.g., zeolitic imidazolate framework) [128]. Generally, surface charge transformation from negative or neutral to positive, or detachment of protective/targeting coating layers aids in improving tumoral penetration and accumulation of the pH-sensitive nanomedicine [129, 130]. It is noted that the acidotic transistor nanomedicine with a pH-sensitive proton transistor can amplify and convert a subtle pH change into sharp membranolytic activities, eliciting a robust tumor-killing effect [131].

Organic nanomedicine. Tumor acidosis-induced aggregation of a nano-assembly could enhance its imaging/therapy performance. For example, a PEGylated porphyrin-peptide-based nanofiber was developed with a negative ζ -potential. It was experimentally confirmed that the imidazole group in the nanomedicine would be protonated in an acidic microenvironment, contributing to an aggregation status by reducing their electrostatic repulsion. The pH-activatable aggregation resulted in strong fluorescence intensity in the tumor for up to 9

days post-treatment and potent $^1\text{O}_2$ generation for effective PDT. This long-term imaging ability was favorable for prognostic monitoring (Figure 4A) [132].

pH-induced disassembly of nanomedicinal structures is readily accomplished in the TME and this strategy is the most widely used for developing pH-activatable nanomedicine. A hollow metallosupramolecular nanocapsule, constructed from the polymerization of boronic monomers and catechol monomers, the incorporation of Fe^{III} via the Kirkendall effect, and the loading of DOX, was applied to realize a cascade pH-activatable PAI-guided photothermal-chemotherapy. Initial tumor acidosis-induced “negative to positive” charge transformation was achieved by a combined effect of reversible phenolic hydroxyl ionization and catechol- Fe^{III} coordination; as the pH value of the buffer changed from 7.4 to 7.0 and then 6.5, this activatable nanocapsule showed a steady increase in the ζ -potential but a negligible change in the size distribution. A second wave of C=N cleavage in the endosome ($\text{pH} < 5.5$) enabled robust release of the encapsulated DOX. The PA intensity reached a peak at 6 h post-injection of this nanocapsule in the MCF-7 breast tumor-bearing mice, and this time point was determined to be optimal for the NIR treatment [134].

Inorganic nanomedicine. pH-induced structural transformation of inorganic nano-assemblies with surface coating modifications (e.g., a mixed-charge zwitterionic surface) contributes to enhanced performances of imaging (T2WI, CT, PAI) and therapy (PTT, PDT, and RT). pH-activatable structural collapse of inorganic nanoparticles, such as the expansion of pores in mesoporous silica, has been

found to promote on-demand sustainable release of drugs and bioactive metal ions, facilitate deep cargo penetration in the tumor tissue, and reduce long-term retention of inorganic nanostructures [135]. In addition, an acidic lysosomal environment in tumor cells was found to facilitate the release of cargos (organoselenium SED-1b and SPIONs) from PLZ4 ligand-modified PLGA nanoparticles (PLZ4@SeD); the SED-1b release rate increased from ~30% to around 80% at 72 h when a pH 5.3 buffer was used. The *in vivo* MR performance was examined in three fresh intact bladders resected from bladder cancer patients in the manner of intravesical instillation of PLZ4@SeD. A time-dependent and tumor-specific slight T2WI enhancement was observed. As demonstrated in the bubble-formation tests and MTT assays, PLZ4@SeD imposed a strong cytotoxicity effect on a few cancer cell lines (EJ, J82, T921, SV-HUC-1, MCF7, and HepG2) in a normoxic environment and exhibited a strong oxygen-generation ability via the Fenton reaction. Moreover, the antitumor therapeutic effect of PLZ4@SeD suggested that it could be a potent ROS nanogenerator and a hypoxia reducer, which were confirmed with EJ cells in various tests (cell migration, cell cycle arrest, apoptosis, and ROS generation) [136]. In another study, a low pH in the lysosomes promoted rapid disintegration of ultrasmall γ -Fe₂O₃ and release of Fe³⁺ ions/DOX from UNA- γ -Fe₂O₃@PP@Dox@PF with an excellent photothermal conversion efficiency (PCE) of 59.85%. This pH-activated disassembly behavior improved the imaging performance with a dynamic T2-T1 MRI change; under a 7.0 T MR scanner, the *in vitro* r_2 and r_1 value of this nanostructure was 146.23 mM⁻¹s⁻¹ and 0.2 mM⁻¹s⁻¹ at pH 7.4, respectively, however, the r_2 dropped to 41.3 mM⁻¹s⁻¹ and the r_1 rose to 0.39 mM⁻¹s⁻¹ at pH 5.5. The anti-tumor effect was confirmed by the synergistic action from the released DOX, a rise in the localized temperature, and the released Fe³⁺ ions. Conversion of Fe³⁺ to Fe²⁺ was accompanied by the generation of •OH under GSH and H₂O₂, leading to chemodynamic therapy, mitochondria damage, and an increase in lipid peroxidation. DOX-induced DNA damage and thermal damage produced by NIR-irradiated UNA- γ -Fe₂O₃ exerted additive tumor-killing effects, contributing to a synergistic antitumor therapy with a tumor inhibition rate of 98.6% [137].

Organic-inorganic hybrid nanomedicine.

Organic coatings often serve as a protective and/or stimuli-activatable layer for an inorganic core in the organic-inorganic hybrid nanomedicine. For example, a pH-activatable polymer was employed as a gatekeeper for reserving manganese (Mn) ions in a

ternary PtWMn alloy via doping multivalent Mn ions (Mn²⁺ and Mn³⁺) to a Pt or W nano-cubic skeleton, to obtain the R-PtWMn nanomedicine. The pH-activatable polymer was protonated in an acidic tumor microenvironment and it underwent a hydrophobic-to-hydrophilic transition. Upon exposure to the stimulus *in vitro*, pH-dependent •OH generation, GSH consumption, oxygen generation, and a high level of ferroptosis were found for R-PtWMn, while negligible changes for Nr-PtWMn, a non-responsive control nanomedicine. Moreover, the released Mn ions from the activatable nanostructure contributed to a rise in the pH-dependent r_1 and r_2 values at 7.0 T MRI, as well as an enhanced imaging contrast in the tumor sites of the 4T1-bearing mice at the first six hours post-injection. The tumor inhibition rate of the R-PtWMn-treated group exceeded that of the Nr-PtWMn-treated group as well as the groups treated with sham (*i.t.*) and sham (*i.v.*). This study suggested that this organic-inorganic hybrid nanomedicine could realize ferroptosis through real-time MR monitoring in a tumor acidosis-activatable manner (Figure 4B) [133]. In another study, partially-released zinc ions from the core in an inorganic nanostructure (microporous ZIF-8 NPs) in response to the tumor acidosis were employed to tune the hydrophilicity and surface charge of a sulfoxide-containing fluorinated homopolymer acting as the coating layer of the nanostructure, resulting in a high level of tumor uptake and pH-activated controlled release of encapsulated DOX which were monitored via ¹⁹F MRI [138].

To note, non-specific pH activation could occur in normal cells since they have an acidic environment in their lysosomes or late endosomes (pH < 5.4). To achieve drug release only in the extracellular tumor microenvironment at a pH of ~6.6, but not inside normal cells, an accelerator/brake strategy was adopted to regulate the optimal pH response. A core-satellite nanomedicine, SPNs@CoOOH, was prepared: semiconducting polymer nanoparticles as the satellite layer, and cobalt hydroxide oxide nanoparticles as the core. A low pH in the extracellular tumor tissue accelerated the release of Co³⁺ ions from SPNs@CoOOH, and the released Co³⁺ ions reacted with H₂O to generate products such as ¹O₂ and H⁺. H⁺ exerted a braking effect towards the chemical reaction to control the release of Co³⁺ ions, and the therapeutic ¹O₂ would activate the thiophene unit in the nanomedicine to generate near-infrared chemiluminescence via chemically electron exchange luminescence. By regulating the percentage of Co³⁺ and the semiconducting polymer, efficient ¹O₂ production and high chemiluminescence signal were realized for chemiluminescence imaging-monitoring,

pH-selective cancer therapy [139].

Taken together, under different tumor acidosis conditions at extracellular, endosomal, or lysosomal locations, the protonation of the pH-sensitive moieties in the polymers and/or the dissociation of inorganic nanostructures contribute to nanostructural transformation, leading to cargo release, aggregation, disassembly, and disintegration. Precisely manipulating the response of chemical moieties to a slight change in the pH is achievable in the organic nanomedicine, thus pH-sensitive drug-conjugated organic nanomedicine is appealing from the aspects of chemistry, manufacture and control (CMC) manufacture processes and biosafety. A systematic study of inorganic nanostructural responses to a broad pH range should be pursued to understand their activatable drug release behavior and imaging/therapy effects. Meanwhile, the impact of long-term retention of these metals or micronutrients (e.g., Fe and Mn ions) in the organs after treatment with inorganic nanomedicine should be carefully investigated.

3.2.2. Redox-activatable theranostic nanomedicine

In the redox-activatable nanomedicine, the breakage of a disulfide bond or other redox-sensitive ligands in response to ROS and/or GSH contributes to an enhanced theranostic performance [140]. Meanwhile, the reaction of bioactive ingredients (metal nanoparticles) in the nanomedicine with redox agents enables “turn-on” imaging, chemodynamic therapy, ferroptosis, immunomodulation, and homeostasis disturbance.

GSH-induced disassembly. One GSH-activatable Fe-Cu@PANI nanoparticle synthesized by doping metal ions (Fe^{3+} and Cu^{2+}) and aniline into a BSA template was prepared and used for PAI-guided PTT. Cu^{2+} in this nanomedicine reacted with abundant GSH in the tumor cells, leading to the formation of an emeraldine salt status of protonated PANI and a redshift to 820 nm for NIR, thus generating a cascade-like enhanced GSH response evidenced with simultaneous PA signal/localized heat. Transmission electron microscopy (TEM) images demonstrated that the size of Fe-Cu@PANI NPs significantly decreased from ~230 nm to 7 nm after incubation with 1.0 mM GSH. *In vivo* PAI further confirmed its GSH-activatable imaging property, as the PA intensity in the tumor area markedly increased after 6 days *i.t.* injection and remained stable on day 12 to day 14. Thermographic images of 4T1 tumor-bearing nude mice revealed that the temperature in the tumor area rose to 55.6 °C in the group treated with Fe-Cu@PANI + 808-nm laser irradiation, while in the group treated with PBS at the

same irradiation condition, the temperature merely reached 40.3 °C, indicating a potent thermal-generation capacity of Fe-Cu@PANI. Furthermore, the relative tumor volume in the Fe-Cu@PANI + laser-treated group shrank to nearly zero on day 16 post-treatment, while it was ~6.5, ~6.5, and ~5 for the group treated with PBS, Fe-Cu@PANI, and PBS + laser, respectively [141].

This GSH-induced disassembly strategy also applies to molecular assembly-based theranostic nanomedicine. Two GSH-activatable molecular structures (1-Zn-PPA and 1-NLG) were prepared by covalently conjugating photosensitizers Zn-PPA-SH or IDO inhibitors NLG919 to the 2-Gd molecular backbone with a disulfide bond, respectively; MRI agents Gd-DOTA, hydrophobic fluorophores AO-Luc, and tumor-targeting ligands cRGD were integrated into the molecular backbone. These two molecular structures self-assembled into a spherical nanoassembly at a size of ≈ 100 nm with a high r_1 value of $18.7 \pm 0.3 \text{ mM}^{-1} \text{ s}^{-1}$ and a quenched fluorescence status. Upon exposure to GSH, the functional molecules were activated or released from the disassembled nanostructure, exerting their therapeutic or imaging effects: a) the FL intensities of AO-Luc at 547 nm and Zn-PPA-SH at 672 nm were markedly enhanced with a ~500- and ~85.9- fold improvement, respectively, b) the released NLG919 inhibited IDO1, reducing immunosuppressive Tregs, and c) the released Zn-PPA-SH could bind to albumin for robust ROS generation upon light/ultrasound stimulation, inducing a direct tumor-killing effect or augmenting immunological cell death. In treating the mice bearing orthotopic 4T1 breast cancer and GL261 glioma brain cancer, the FL/MR bimodal signal-guided synergistic sonodynamic and photodynamic therapy showed a remarkable tumor suppression rate, a robust immunogenic cell death (ICD)-mediated immune response, and an extended survival time [142].

GSH-mediated reduction of Pt(IV) prodrugs to active Pt(II) drugs is a typical example of redox-induced activation of nanomedicine for cancer theranostics [143]. The use of a Pt(IV) prodrug-derived nanostructure with imaging moieties could improve the bioavailability of Pt(II) and enable imaging-assisted therapy. For example, a MnO_2 -Pt(IV) nanomedicine prepared by the one-pot ultrasonication method was reduced to Mn(II) and Pt(II) in tumor cells. These released metal ions exerted a ~4-fold cytotoxic effect against A549 cells over the Pt(IV) precursor, meanwhile, a ~2.4-fold T1-MRI enhancement was achieved at *in-vivo* tumor sites compared to MnCl_2 [144]. Another single molecule-assembled Pt(IV) prodrug was prepared by

incorporating methylene blue, a photosensitizer, and quinone methide (QM), a GSH-depleting adjuvant, in the hydrophobic domain of the prodrug. In this design, both Pt(IV) and QM were dedicated to disrupting the cellular GSH-defense system, indirectly boosting therapeutic effects from methylene blue-mediated PDT and Pt(II)-mediated chemotherapy. *In vivo* fluorescence imaging mediated by GSH-activated methylene blue revealed peak accumulation of this prodrug nanomedicine at 8 h post-injection [145]. In another study, a nanomedicine with a simple structure, Bio-I-Pt, was developed via conjugating iodine and biotin to a Pt(IV)-based small molecule in which the Pt and I content was 47.1% and 36.1%, respectively. This molecule self-assembled into spherical nanoparticles at a size of around 100 nm with a high X-ray attenuation efficiency. After internalization of the spherical nanostructure into cellular cells at a high GSH concentration via biotin-receptor interaction, Pt(IV) in the nanomedicine was reduced to Pt(II) for chemotherapy and I_3^- generated from reduction helped reduce Bcl-2, thus reverting Pt-based drug resistance. After incubation with reductive sodium ascorbate for 12 h, the Pt and iodine release rates were 73.2% and 73.9%, respectively, while in the buffer without the reductant, the accumulative release ratio for Pt and iodine was 28.8% and 24.4%, respectively. TEM images suggested distinctive dissociation of the spherical nanostructure under reductive conditions. CT images of the Bio-Pt-I-treated tumor-bearing mice helped delineate the tumor area at a high density at 12 h post-intravenous injection. Western blotting results confirmed that the Bcl-2 expression intensity was 0.97 and 1.72 in the saline-treated A549 and A549/DDP cells, while the intensity sharply dropped to 0 and 0.1 in the A549 and A549/DDP cells after Bio-Pt-I intervention, respectively (Figure 5A) [146].

GSH-induced assembly. Gold nanoparticles coated with a GSH-sensitive layer are one representative nanomedicine with GSH-induced aggregation. A DNA sequence with a disulfide bridge was connected to G-quadruplex-hemin or G-quadruplex-Ce6 with AuNPs modified with a thiolated capture probe to construct Au-GH-dsDNA-DOX and Au-GC-dsDNA-DOX, respectively, after DOX was loaded onto the AuNPs. Under a reductive environment, the disulfide bridge in double-stranded DNA was broken to induce cargo release and AuNPs aggregation. GSH-triggered AuNPs aggregation after GSH intervention, which was ascribed to the hybridization of the exposed end of the capture probe, was verified through the following observations: the aggregates in the TEM images; a remarkable size increase from ~25 nm to

~500 nm in the DLS diagram; a red shift in the absorption spectra; and a dramatic temperature rise in response to light irradiation [147]. It was also reported that mPEG-CONH-ss-NH₂ was introduced to a polydopamine coating shell of AuNPs to form Au@PDA-ss-PEGm NPs, and the NPs without disulfide bonds were used as a control. Upon GSH stimulation, long-chain PEG was detached and naked Au@PDA NPs aggregated due to an imbalance in the surface charge caused by a high-concentration of salt ions. These GSH-triggered nanoaggregates helped display enhanced PA images and plasmon coupling enhanced the photothermal effect. The peak of the PA intensity in the tumor area treated with this activatable nanostructure had a 7.2-fold increase at 32 h post-injection, while there was no significant signal change in the groups treated with PBS and the NPs without the disulfide bonds. Meanwhile, a distinctive temperature rise of 38.9 °C was seen in the tumor area of the HeLa tumor-bearing mice treated with the activatable nanostructure plus laser irradiation, leading to a remarkable tumor inhibition rate, while negligible changes in the thermal imaging signal and no tumor growth inhibition were seen in the control groups (Figure 5B) [148].

ROS-induced disassembly. In response to an elevated ROS level in tumors, the most common activatable result is the disassembly of the nanomedicine, while inorganic nanostructures may perform a similar catalysis function as catalase. For example, a fluorescent probe Ag₂S QDs and tellurium (Te) nanorods were prepared via a polypeptide PC₁₀AGRD-assisted biomimetic method and then coated with extracted 4T1 tumor cell membranes to form the cancer cell membrane-coated Ag₂S QDs and Te nanomedicine (abbreviated as CCM@AT). The NIR-II FL emission of Ag₂S QDs was quenched by Te nanorods in the prepared nanomedicine. Meanwhile, the dissociation of TeO₆⁶⁻ from the Te nanorod upon stimulation with a high H₂O₂ level triggered a switch-on for NIR-II imaging by Ag₂S QDs; meanwhile, the released TeO₆⁶⁻ and the exposed Ag₂S QDs synergistically exerted a combined effect of chemotherapy and photothermal therapy. *In vivo* FL imaging of the 4T1 tumor-bearing mice displayed the tumor-specific distribution of CCM@AT, while multi-organ distribution (liver and spleen) of the nanostructures without the Te nanorod indirectly indicated the vital role of the redox-activatable Te nanorod. As a consequence, the treatment with CCM@AT and laser outperformed other treatments, with a high tumor inhibition rate of 98.4% in comparison with 65.3% for CCM@AT without laser, 68.9% for CCM@T, and 86.9% for CCM@A and laser [149].

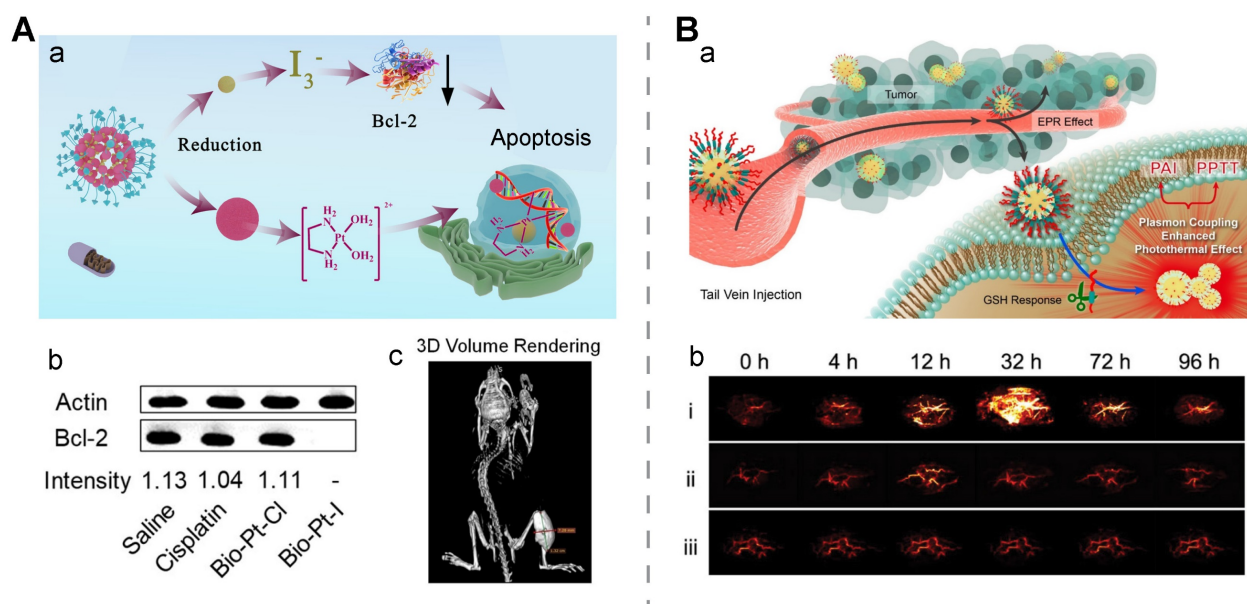


Figure 5. GSH-activatable nanomedicine for cancer theranostics. A) GSH-activatable iodine-conjugated Pt(IV) nanomedicine (Bio-Pt-I) for computed tomography-guided chemotherapy. a) Schematic of Bio-Pt-I design. b) Western blots of Bcl-2 expressed in tumors after various treatments. c) 3D volume-rendering CT images of PDX tumor models injected with Bio-Pt-I. Reproduced with permission [146]. Copyright 2022, American Chemical Society. B) A GSH-activatable nanoprobes for photoacoustic imaging and photothermal therapy. a) Schematic design of the nanoprobes. b) PAI images of tumor sites treated with the nanoprobes (i), Au@PDA-PEGm NPs (ii), and PBS (iii) at different time points. Reproduced with permission [148]. Copyright 2022, American Chemical Society.

Redox-triggered disassembly of organic nanomedicine could result in a “turn-on” of optical imaging due to the disruption of aggregation-caused quenching or Förster resonance energy transfer. A fluorescently traceable prodrug nanomedicine was prepared by bridging zwitterionic fluorescent rhodamine (RhB) with chemotherapeutic camptothecin (CPT) via a disulfide bond. Interestingly, the responsiveness of the nanomedicine towards both H_2O_2 and GSH was verified with a rapid fluorescence enhancement was observed at the condition of ≥ 100 mM H_2O_2 and ≥ 10 mM GSH. With the aid of this redox-cleavable linkage, a high tumor inhibition rate of 77.4% was achieved in comparison with 51.2% in the free CPT-treated group, meanwhile, the highest fluorescence intensity was found at tumor sites at 12 h post-injection [150]. In another report, a ROS-activatable chemotheranostic prodrug nanomedicine (Bio-(8)-MB-CPT) was developed by conjugating a ROS-responsive leucomethylene (LMB) derivative to a self-immolative space-containing biotin-camptothecin conjugate. Upon exposure to ROS, LMB was converted to methylene blue fluorophores to turn on NIR imaging and CPT was released from the nanomedicine. Fluorescent imaging mediated by activated methylene blue showed a similar detection ability as ultrasonography for tracking cervical cancer abdominal metastases at different stages in murine tumor models. As shown in high-performance liquid chromatography (HPLC) results, this nanosystem exhibited a drug release efficiency of up to 92.04% after incubation with 5.0 equivalents of HOCl.

Accordingly, this Bio-(8)-MB-CPT nanomedicine displayed a high tumor inhibition rate of 99.9% in treating metastatic cervical cancer and no abdominal metastases sites were found through monitoring via ultrasonography (Figure 6A) [151].

ROS-induced on-site activation. Fusing ROS-activatable (scavenging) imaging agents into therapeutic T cells is a nanoengineering strategy to realize imaging-guided immunotherapy (Figure 6B). A fusogenic liposome modified with $\alpha CD3$ and 2,2,6,6-tetramethylpiperidine (TEMP) moieties was employed to target and fuse with T cells to produce the nanomedicine T-Fulips, and Iso-Fulips without the targeting function was set as a control. Upon stimulation by the tumoral ROS, the TEMP groups were oxidated into paramagnetic 2,2,6,6-tetramethylpiperidine 1-oxyl (TEMPO) radicals, neutralizing ROS for restoring the T cell function and allowing MRI for real-time monitoring. *In vitro* T_1 images supported that the imaging contrast of the T-Fulips solution was substantially elevated after co-incubation with H_2O_2 at an increased concentration; the imaging contrast in the T-Fulips solution with 50 μM H_2O_2 was improved two times higher than that of the control group with Iso-Fulips. Flow cytometry analysis suggested upon the treatment with H_2O_2 , the surface -SH groups on the T cells in the presence of T-Fulips was reduced from 21.5% to 14.1%, while it remained to be 29.7% in the group of H_2O_2 + Iso-Fulips. Moreover, the proliferation capacity of T cells was restored in the presence of T-Fulips. Under oxidative stress induced by X-ray, the presence of T-Fulips increased the

number of CD4⁺ cells, CD8⁺ cells, and -SH⁺ cells in the tumor slices. These experiment results suggested T-Fulips could enhance T cells activity by regulating the -SH surface groups. The radiation therapy-treated 4T1 tumor-bearing mice were used to examine the role of T-Fulips in alleviating oxidative stress based on the visible T cells activity. Compared to Iso-Fulips without the T cells-targeting function, the presence of T-Fulips contributed to a much significant increase in the T1 signal change in the tumor area, a rise in the percentage of effector T cells (CD45⁺CD4⁺IFN- γ ⁺, CD45⁺CD8⁺IFN- γ ⁺, CD45⁺CD4⁺IFN- γ ⁺SH⁺, and CD45⁺CD8⁺IFN- γ ⁺SH⁺), as well as a superior tumor growth suppression effect. Additionally, an enhanced therapeutic outcome of adoptive T-cell therapy was seen with the aid of T-Fulips in the B16F10-OVA tumor-bearing mice. To conclude, this nano-fusion strategy in response to ROS was able to achieve both alleviating the oxidative stress and realizing real-time monitoring of T cells activities [152].

In addition to triggering drug release or activating imaging at a high tumoral redox level, modifications of the organic or inorganic nanostructures were explored to consume or covert

excess redox agents, contributing to chemodynamic therapy, glutathione depletion-enhanced ferroptosis, and oxidative stress relief. Immune checkpoint inhibitors (ICIs)-based immunotherapy recently enjoys a flourishing boom, however, the potential detrimental effect of tumoral reductive agents on ICIs remains to be revealed. It is hypothesized that the disulfide bond of antibodies may be broken after exposure to GSH, resulting in a collapse in the ICI hierarchical structure. In this context, the nanoengineering approach could be explored to address the redox stress to aid in immunotherapy. Furthermore, it is encouraged to develop redox-activatable imaging for real-time monitoring of immunotherapeutic agents or cells.

3.2.3. Enzyme-activatable theranostic nanomedicine

Over-expressed or tumor-specific enzymes are located at different sites of the tumor microenvironment. Utilization of these enzymes to prepare enzyme-activatable theranostic nanomedicine offers site-specific release or activation of therapeutic/imaging agents.

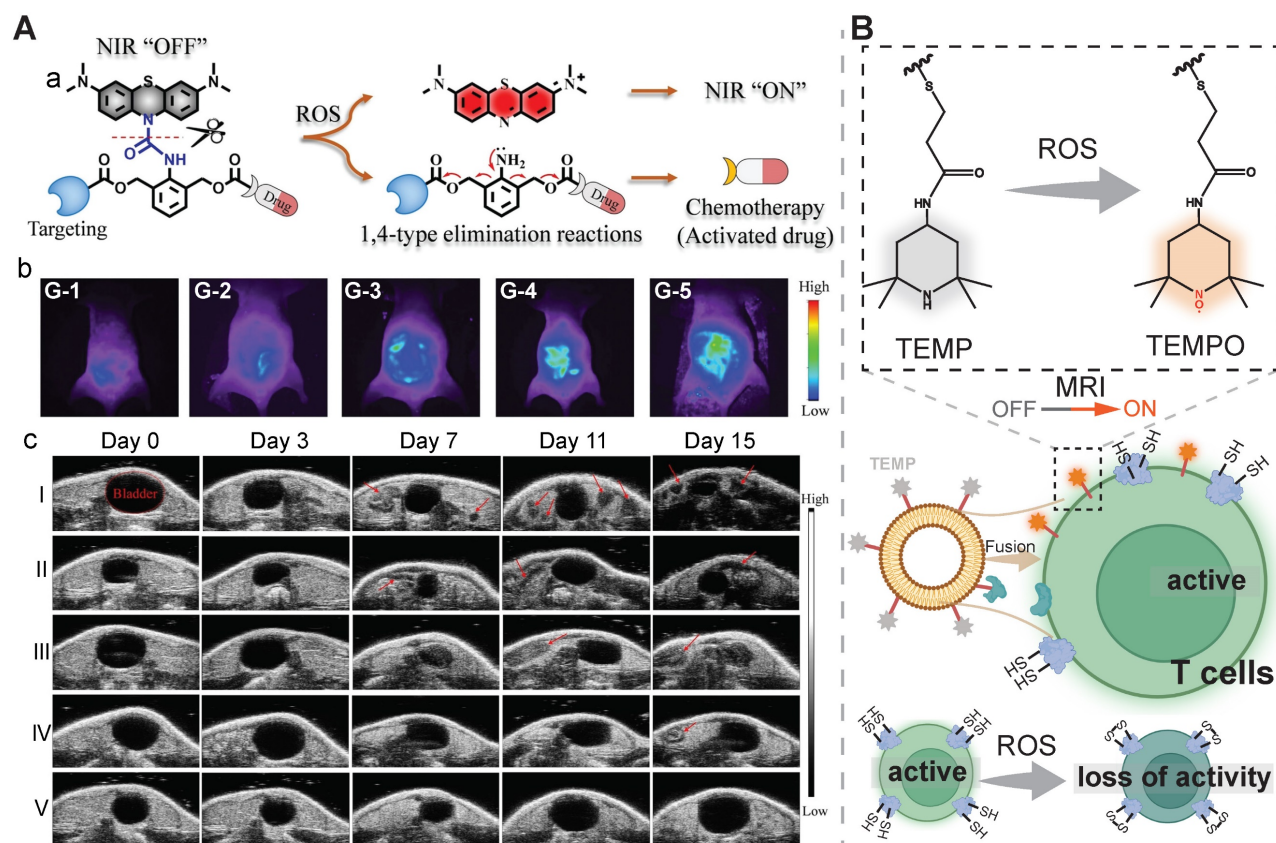


Figure 6. ROS-activatable nanomedicine for cancer theranostics. A) An ROS-activatable prodrug nanomedicine for chemotherapy and NIR imaging of cervical cancer metastases. a) Illustration of ROS-activated disassembly of the prodrug nanomedicine. b) Fluorescence images of cervical cancer metastases at different stages with the aid of this nanomedicine. c) Long-term ultrasound imaging of the mice treated with different formulations (I: saline; II: free CPT; III: (4)-MB-CPT; IV: (8)-MB-CPT; V: Bio-(8)-MB-CPT). CPT: camptothecin; MB: methylene blue; Bio: biotin. Reproduced with permission [151]. Copyright 2022, Wiley-VCH. B) ROS-induced on-site activation for immunotheranostics. 2,2,6,6-tetramethylpiperidine (TEMP)-modified liposome was fused with T cells via active targeting. When these fused T cells were exposed to an elevated ROS level in the TME, the TEMP on the liposome surface was oxidized to TEMPO. This procedure scavenged intracellular ROS to restore the antitumor activity of T cells and enable a turn-on of MRI imaging for monitoring the therapeutic response. The figure was created with BioRender.com according to the hypothesis presented in Ref [152].

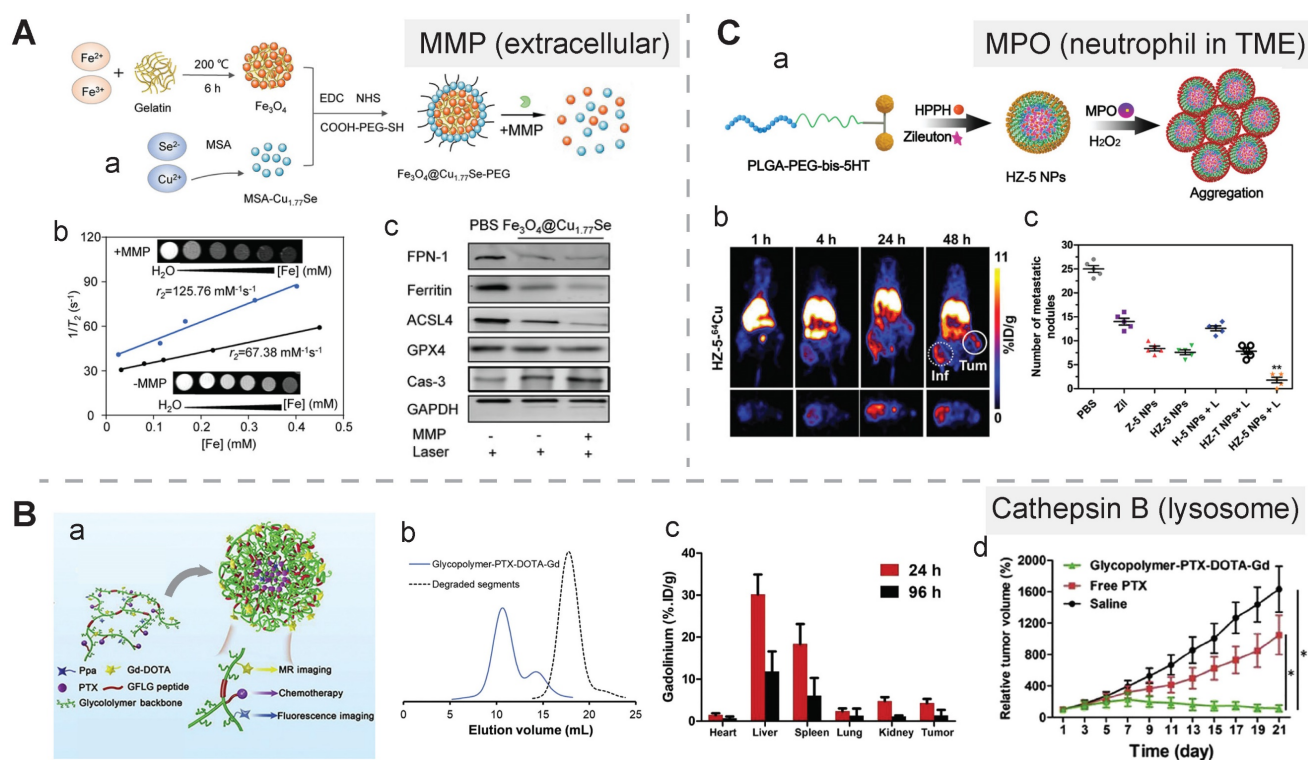


Figure 7. Enzyme-activatable nanomedicine for cancer theranostics. A) MMP2-induced disassembly of a nanomedicine for PAI, MRI, and photothermal ferroptosis therapy. a) Schematic of the fabrication of the nanomedicine and its disassembly in response to MMP2. b) T2-weighted MR images and corresponding plots of the nanomedicine incubated with or without MMP2. c) Western blots analysis of ferroptosis- and apoptosis-related protein expression in 4T1 cells after different treatments. Reproduced with permission [153]. Copyright 2022, Wiley-VCH. B) Cathepsin B-induced degradation of gadolinium-labeled branched glycopolymer-PTX conjugates for MRI, fluorescence imaging, and chemotherapy. a) Schematic design. b) Size-exclusion chromatography profiles for this conjugate before and after incubation with cathepsin B. c) Distribution of this conjugate in major organs determined by the gadolinium retention. d) Tumor growth curves after different treatments. Reproduced with permission [154]. Copyright 2021 the Authors, published by Elsevier B.V. C) Myeloperoxidase-induced aggregation of HZ-5 NPs for neutrophil-targeting PDT or PET. a) Schematic of the aggregation process of HZ-5 NPs. b) PET images of 4T1 tumors after *i.v.* injection of ^{64}Cu -labeled HZ-5 NPs. c) The counts of lung metastatic noduli in the mice treated with different methods. Reproduced with permission [155]. Copyright 2020, Wiley-VCH.

Extracellular location. The matrix metalloproteinase (MMP) family constitutes the majority of extracellular enzymes in the tumor site. Gelatin was selected as an MMP-2 activatable linker in a theranostic nanomedicine which could be disassembled in response to the extracellular enzyme. In this study, gelatin as a mediator was mixed with Fe^{3+} ions to form interlaced Fe_3O_4 aggregates under 200°C , and the aggregates were subsequently conjugated with $\text{Cu}_{1.77}\text{Se}$ and modified with a PEG coating layer, resulting in the $\text{Fe}_3\text{O}_4@ \text{Cu}_{1.77}\text{Se}$ -PEG nanomedicine with a photothermal conversion efficacy of 67.6%. MMP-2 induced distinctive disassembly of this nanostructure, and its size significantly shrank from 124.2 nm to 14.6 ± 6.9 nm, which was accompanied with an elevated level of T2 MRI contrast, an increase in the r_2 value from 67.38 to $125.76 \text{ mM}^{-1}\text{s}^{-1}$, and an enhanced photothermal therapeutic effect due to deep penetration and an improved ferrotherapeutic efficacy. Additionally, the synergistic antitumor effect, which was due to PTT-induced caspase-3-mediated apoptosis, escalated Fenton reaction-mediated ferroptosis induced by released $\text{Fe}^{3+}/\text{Cu}^{2+}$, and immunomodulation induced by apoptosis and

ferroptosis (polarizing TAMs and inducing ICD), led to effective control of both primary and distant tumors. After photoirradiation of primary tumors, the relative tumor volume in the $\text{Fe}_3\text{O}_4@ \text{Cu}_{1.77}\text{Se}$ -PEG-treated mice was reduced to nearly zero, while it was ~ 8 , ~ 5 , and ~ 2.5 in the group treated with PBS, Fe_3O_4 , and $\text{Cu}_{1.77}\text{Se}$, respectively. Photoirradiation was also applied to distant tumors, and the tumor-bearing mice group treated with $\text{Fe}_3\text{O}_4@ \text{Cu}_{1.77}\text{Se}$ -PEG displayed a remarkable decline in the relative tumor volume, and the volume was 3.9-, 3.0-, and 1.8-fold lower than that in the group treated with PBS, Fe_3O_4 , and $\text{Cu}_{1.77}\text{Se}$, respectively. Besides, a significant drop in the MRI intensity in the tumor site indicated this nanoprobe could spatially-temporally monitor the therapeutic process (Figure 7A) [153].

In addition to activation of nanomedicine by MMP2, MMP9 is often harnessed to prepare activatable organic coatings for inorganic nanomedicine. For instance, an MMP9-activatable peptide-containing polymer, PIX-(GPLGL-PEG) $_2$ (abbreviated as PMP), was employed to encapsulate DOX and ultrasmall superparamagnetic iron oxide (USPIO),

resulting in the PMP@USPIO/DOX nanomedicine through a self-assembly process. Upon exposure to MMP9, this nanostructure was disassembled and the imaging power was switched on. Thus, this nanostructure could be used to quantify the MMP level and monitor the drug release process [156]. Another surface modification strategy by applying an MMP-9 activatable zwitterionic tetrapeptide, EG₈-GPKGLRGD-EG₅-C, was recently proposed to promote self-assembly of gold nanoparticles. The remaining RGD sequence after enzymatic cleavage facilitated self-assembly of gold nanoparticles with a size of 585 ± 19 nm via electrostatic interaction, which was confirmed from the TEM images of MMP9-containing NPs and MDA-MB-231 tumor cells after incubation with the gold nanoparticles [157].

Cellular surface and intracellular location. A group of tumor-associated enzymes are over-expressed on the cellular membrane surface or in the intracellular environment. Our group has devoted to the development of cathepsin B-responsive biodegradable theranostic nanostructures via a tetrapeptide GFLG linker. We have prepared a biodegradable branched polymeric nanoparticle, pHPMA-PTX-Gd-Cy5.5, in which cathepsin B-activatable linkers were installed on the pHPMA backbone and at the conjugated site of PTX. Size-exclusion chromatography (SEC) profiles of this nanostructure incubated with cathepsin B for various time points revealed that the molecular weight of this nanostructure remarkably dropped from 186 kDa to 25 kDa, and the PDI from 2.30 to 1.2, at 12 h post-incubation, while in the PBS-incubated group, the MW and PDI values remain unchanged, indicating cathepsin B could successfully induce the degradation of the nanostructure into small fragments for renal excretion. Conjugation with a fluorescent molecule, Cyanine 5.5, and an MR agent, gadolinium chelates, offered dual-modal imaging which helped reveal the biodistribution of the nanomedicine, monitor the processes of cellular internalization, vascular extravasation, and tumor penetration, as well as assess its tumor accumulation and evaluate its therapeutic efficacy. Moreover, the conjugated PTX could be released specifically triggered by cathepsin B, which was confirmed from the HPLC, and the released PTX decreased the tumor cell viability, damaged the microfilaments (α/β tubulin and p-actin), and induced apoptosis. In this study, the T1 value in the tumor area determined by T1 mapping was used for three-week monitoring of the therapeutic outcomes after various treatments [158]. Next, we prepared another cathepsin B-activatable gadolinium-labeled branched glycopolymer-PTX by following the prior design concept of biodegradability.

The SEC profiles indicated that after co-incubation with cathepsin B, the nanostructure (MW = 244 kDa, PDI = 2.48) was shattered to renal-excretable fragments (MW = 28 kDa, PDI = 1.26). Meanwhile, this nanostructure had an improved antitumor efficacy (tumor growth inhibition (TGI): 90.6%) and an enhanced MRI performance ($r_1 = 7.1 \text{ mM}^{-1}\text{s}^{-1}$, the peak of the relative enhanced signal intensity (SI) in the tumor: 275%) in contrast to the previous one (TGI: 81.3%, $r_1 = 8.6 \text{ mM}^{-1}\text{s}^{-1}$, the peak of SI in the tumor: ~230%) (**Figure 7B**) [154]. These studies validate the feasibility of using GFLG peptides as a cathepsin B-activatable linker and provide insights into the design of enzyme-activatable polymer-drug conjugates for theranostic application [159].

Moreover, sequential enzyme activation strategy, a dual-lock activation approach for more specific drug release or a sequential turn-on of the imaging function, has been proposed for developing nanomedicine for cancer theranostics. This strategy was demonstrated by a recent study with a theranostic probe, PLCy, which was prepared by conjugating PEG to a mitochondria-targeting NIR fluorophore, hemicyanine (CyNH₂), via an acetylated lysine Boc-Lys(Ac)-OH group sensitive to two enzymes. The theranostic function of CyNH₂ was masked via a twisting intramolecular charge transfer effect. Sequential stimulation by histone deacetylase and cathepsin L assisted in the detachment of PEG and exposure of CyNH₂, leading to a switch-on of fluorescent imaging of tumor cells and exertion of the NIR phototoxicity on mitochondria, respectively [160].

TME-infiltrated neutrophils. Neutrophils-associated enzyme activation strategy applies to the design of cancer nanomedicine for theranostics, which may be helpful in the case of cancer-associated inflammation. The example for this strategy was demonstrated with myeloperoxidase (MPO) in neutrophils as a targeting biomarker and an endogenous stimulus for triggering nanoparticle aggregation. The ligand modified with two 5-hydroxytryptamine ends, abbreviated as bis-5HT, reacted with MPO to produce radicals that could bind to other residues for prolonged retention of bis-5HT in the neutrophils. To apply bis-5HT to theranostics of neutrophils, it was conjugated to PLGA-PEG-COOH in which a leukotriene inhibitor, zileuton, and a photosensitizer, HPPH, were encapsulated, resulting in activatable HZ-5 NPs. Upon co-incubation of HZ-5 NPs with a MPO buffer or 4T1 cells, nanoaggregates could be seen in the TEM images and confocal images, and an increase in the size from 105 ± 15 to 246 ± 33 nm in the DLS diagram. To perform imaging-guided

therapy, ^{64}Cu -labelled HZ-5 NPs reached the highest level of tumor accumulation at 24 h post-injection, and this time point was determined to be an optimal time for performing PDT. Moreover, the uptake of these theranostic nanoagents increased from 4.8 to 7.7 ID g^{-1} after the PDT intervention, indicating its auxiliary function was to monitor PDT-induced cancer inflammation. Moreover, neutrophil-induced lung metastasis was effectively inhibited in the tumor-bearing group treated with HZ-5 NPs + laser, confirmed by FL images in the mice and photographs of the excised lung tissues (**Figure 7C**) [155].

Overall, the theranostic effects of the enzyme-activatable nanomedicine rely on the location of enzymes, either forming a self-assembly nanoaggregate or inducing disassembly of its nanostructure. In addition, it is worth noting that the biological function of enzymes that are actively involved in the therapy (e.g., PDT, PTT, and RT) should be carefully identified and their corresponding activatable ligands could be constructed for specific theranostic performance.

3.2.4. Other endogenous stimuli-activatable theranostic nanomedicine

Hypoxia confers drug resistance to various cancer therapies, and it emerges as a potential theranostic target. Ideally, a hypoxia-activatable theranostic agent should aid in monitoring the therapeutic response of hypoxia-activatable prodrugs by real-time delineating the hypoxia area and indicating the hypoxia degree. In one study, a chemotherapeutic CPT drug was connected to boron dipyrromethene (BODIPY), a fluorescent photothermal sensitizer, via a hypoxia-responsive azobenzene linker, forming a heterotrimer prodrug BAC. A hypoxia-activatable theranostic nanostructure, HSA@BAC, was prepared after loading BAC into human serum albumin (HSA). In this nanostructure, fluorescent emission of BODIPY was quenched by CPT via fluorescence resonance energy transfer (FRET). Upon exposure to overexpressed azoreductase in the tumor hypoxia area, this nanostructure was disassembled to release the CPT drug and turn on fluorescence imaging, which provided guidance for precise, localized light irradiation [161]. A dual-emissive Pt^{II} metallacage with hypoxia-activated red phosphorescence and steady blue fluorescence was coated with an amphiphilic diblock copolymer (mPEG-*b*-PBLG) to act as a hypoxia-activatable theranostic nanoagent. Heterologation directed self-assembly of Pt^{II} -*meso*-tetra(4-carboxyphenyl)porphine as an oxygen-sensitive phosphorescent ligand, 9,10-di(pyridin-4-yl)anthracene that emits blue fluorescence, and a Pt^{II}

acceptor to form an activatable metallacage. After incubation of the mPEG-*b*-PBLG-coated metallacage with 4T1 cells under normoxia and hypoxia conditions, a significant enhancement of up to around 450% in red phosphorescence and an increased red/blue emission ratio from 0.224 to 0.886 were observed in the confocal laser scanning microscopy (CLSM) images of the hypoxia-treated cells. Meanwhile, three agents including the Pt^{II} metallacage, the mPEG-*b*-PBLG-coated Pt^{II} metallacage, and free cisplatin were demonstrated to exert similar cytotoxicity towards 4T1 and A549 cells. However, high tumor accumulation of mPEG-*b*-PBLG-coated Pt^{II} metallacage contributed to a better and safer antitumor performance compared to free cisplatin, which was indicated by blood biochemistry tests, body weight measurements, and tumor volume changes [162].

Biological gasotransmitters, such as CO, NO, and H_2S , may be overexpressed in the disease sites. These gasotransmitters may aid in the transformation of the nanomedicine for an enhanced therapy/imaging effect. For instance, intratumoral hydrogen sulfide (H_2S) has been reported to convert AgNPs into Ag_2S NPs, which exerted a photothermal effect for therapy and offered near-infrared imaging [50], or react with Fe^{3+} ions released from a nanostructure to produce Fe_{1-x}S for MRI-guided PTT [163]. One H_2S -activatable theranostic nanoagent exhibited NIR conversion from 1070 nm to 720 nm and ratiometric PA signal responsiveness with stable PA_{680} signal and weakened PA_{900} signal upon H_2S stimulation. During this activation process, fluorophore ZM1068-NB was converted into ZM1068-Ketone with the consumption of H_2S . Furthermore, the depletion of H_2S combined with the photodynamic effect of activated ZM1068 contributed to the improved antitumor performance in a colorectal tumor-bearing mice model via apoptosis [164].

Taken together, the over-expressed or specifically-produced agents in tumor cells can be leveraged as endogenous stimuli for developing activatable nanomedicine for cancer theranostics. The responsiveness of the activatable linkers towards these stimuli could be dramatically different due to the preparation procedure of the nanomedicine, the stimuli type, and the constitutional components of the tumor microenvironment. A couple of activatable linkers for the same stimulus should be evaluated for the nanomedicine, particularly drug-polymer nanoconjugates, and the variations in the responsiveness should be unveiled after the application of the nanomedicine to human- or murine-derived cancer cell lines and their corresponding animal models.

3.2.5. Exogenous stimuli-activatable theranostic nanomedicine

Exogenous stimuli (light, ultrasound, magnetic field, X-ray) as physical forces or activation sources have the advantages of spatial and remote control for activating cancer theranostics [165, 166]. More importantly, radiosensitizers/photosensitizers/sonosensitizers/photothermal agents with a high conversion efficiency are preferred because the drug dosage and the exogenous stimuli dosage could be significantly reduced. To note, exogenous physical stimulation via mechanical forces (compression, tension, shear force, and torque) could aid in cancer therapy by enhancing vascular permeability, imposing mechanical stress on the TME, or transiently relieving the blood-brain barrier [167].

Light. Light directly triggers drug release, activates PDT/PTT agents, or enables PAI. In this context, FLI-guided PDT and PAI-guided PTT have been realized. The optimal duration for light irradiation is usually determined by the time to reach the highest tumor accumulation of the nanomedicine, indicated by imaging signal or contrast.

It has been reported that oxygen is heavily consumed during a photodynamic therapeutic procedure, leading to a hypoxia environment. This finding was utilized to prepare a light-activatable immune adjuvant, denoted as LIA. In this design, PDT-induced hypoxia could aid in the structural transformation of the nanomedicine for eliciting *in situ* vaccination. The loaded chlorin e6 (Ce6)

simultaneously acted as a photodynamic agent for therapeutic function and a fluorescent indicator for assessing tumor accumulation. Ce6-mediated PDT was utilized to damage tumors to release antigens, meanwhile, tumor hypoxia induced by oxygen consumption during PDT aided in transforming the 2-nitroimidazole group in dendrimers to 2-aminoimidazole, exerting an rHAD-mediated adjuvant effect. The reduced oxygen concentration and an increased phosphorescence lifetime or a boosted Singlet Oxygen Sensor Green (SOSG) intensity confirmed the hypoxia environment induced from the combined treatment with LIA and laser irradiation. TEM images revealed time-dependent structural collapse of LIA upon exposure to light, supporting its light-activatable disassembly behavior. Furthermore, in a 4T1 residues-bone marrow-derived dendritic cells (BMDCs) co-incubation model, a nearly two-fold increase in the mature CD80⁺CD86⁺ BMDCs was seen in the group after the treatment with LIA and light irradiation. While there was no change in the number of mature CD80⁺CD86⁺ BMDCs in other treatment groups, including PBS, free Ce6, and Ce6-containing DSPE-PEG_{2k}, with or without light irradiation. Transcriptomic analysis and molecular docking experiments suggested the rHAD-induced DC maturation was realized via the toll-like receptor 7 (TLR7) pathway. Consequently, this light-activated theranostic nanoagent exhibited a superior therapeutic efficacy on primary tumors, abscopal tumors, and rechallenged tumors (Figure 8A) [168].

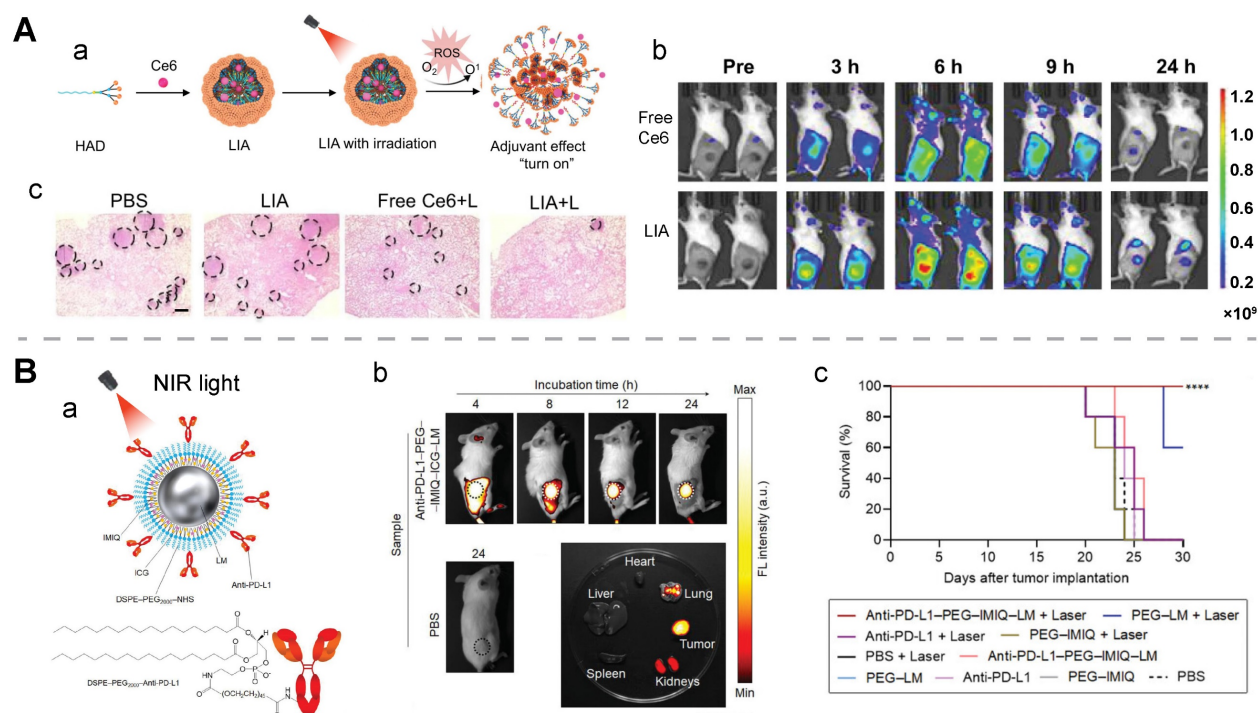


Figure 8. Light-activatable nanomedicine for cancer theranostics. A) A light-activatable amphiphilic dendrimer, LIA, as a fluorescence imaging-assisted immunological adjuvant. a) Schematic of the procedure for preparing LIA and triggering its adjuvant function. b) Fluorescence images of 4T1 tumor models treated with free Ce6 and LIA. c) H&E staining

of lung tissues after different treatments, and black circles represented metastatic nodules, scale bar: 500 μm . Reproduced with permission [168]. Copyright 2021 the Authors, published by Springer Nature. B) A light-responsive liquid metal (LM)-based immunostimulator for NIR-light triggered PTT and release of immunomodulators (anti-PD-L1 and imiquimod (IMI)). a) Scheme for preparation and structure of anti-PD-L1-PEG-IMI-ICG-LM. b) Fluorescence images of CT26-bearing mice and their resected organs after injection of this theranostic nanomedicine. c) Survival rates of the murine tumor model after different treatments. Reproduced with permission [169]. Copyright 2023, published by Wiley-VCH.

In addition to activating PAI and inducing PTT, NIR light functions as a drug-release trigger on photothermal nanoagents. In one study, Ag_2S QDs and chemotherapeutic DOX were camouflaged by macrophage-derived extracellular vesicles via electroporation. NIRF imaging of the tumor-bearing mice treated with this camouflaged nanostructure revealed a duration of 24 h to reach a peak in its tumor accumulation, and the amount of the nanostructure in the tumor was determined to be 16.5% ID/g by inductively coupled plasma mass spectrometry (ICP-MS) analysis. Notably, light in this case was a potent trigger for drug release and structure decomposition. Upon 808 nm light irradiation, the accumulative release of both drugs was significantly improved: the DOX release rate increased from 9.6% to 58.5%, and the QDs release rate rose from 2.1% to 47.0%. Treatment with the light-activated nanomedicine resulted in a high tumor inhibition rate of 86% and an Ag_2S QDs clearance efficiency of > 90% [170]. In another study, NIR-II light acted as a trigger to release carbon monoxide (CO) from Pd@PdCO-MOF, a photo-activated theranostic agent which was composed of a porphyrin-palladium MOF shell and a palladium nanosheet core. Its PCE was found to be 44.6% *in vitro*. The CO release result revealed that the release amount reached a peak value of 14 μM after 1 h light irradiation, and the fluorescent intensity of COP-1 (a CO fluorescent probe) in the CLSM images of 4T1 cells substantially increased with an increase in the irradiation time in the first 10 minutes. The released CO gas was found to enhance PTT through decreasing the ATP level, downregulating HSP expression, and upregulating the expression of cyto C [171]. Similarly, NIR light was reported to induce the release of immunomodulators (anti-PD-L1 and imiquimod) and fluorescent molecules from eutectic gallium-indium liquid metal nanoparticles, a potent PTT agent with a PCE of 47%. During the FL-guided photothermal immunotheranostics of a murine colon cancer model, the treatment with the light-activatable nanomedicine + laser exhibited a superior tumor control rate (nearly complete control) and a significantly higher survival rate than other treatments including PBS, PEG-LM, anti-PD-L1, PEG-IMI, and their combination with laser. Statistically, the survival rate of the CT26-bearing mice group treated by this light-activatable nanomedicine + laser reached 100%, while the survival rate dropped to 60% in the group treated

with PEG-LM + laser and 0% for the other groups (Figure 8B) [169]. Another study further confirmed light-activatable drug release from a photothermal immunotheranostic nanomedicine, AuPB@PDA/Mn. The immunomodulator Mn^{2+} ions were loaded in the polydopamine coating of plasmonic gold blackbody. And upon NIR-II-light, Mn^{2+} ions were discharged by local hyperthermia generated by AuPB@PDA [105].

Overall, light is commonly used as an exogenous stimulus in the cancer theranostic application. Nanostructures with a NIR-II light (1000-1700 nm)-activated photothermal and photoacoustic performance could be explored to address the issue of poor tumor penetration by routine light therapy. Moreover, the photothermal or photodynamic conversion efficiency of a nanostructure is essential for the therapeutic outcome of the nanostructure-derived nanomedicine. Various design strategies on the nanostructure, such as engineering of dual-acceptor semiconductor polymers and modulating donor/acceptor groups, have been exploited to improve the conversion efficiency and imaging performance [172, 173]. In addition, Janus-like PTT NPs were reported to significantly increase local temperature than conventional ones due to their thermophoresis effects [174], and the generated heat gradients could drive Janus-like NPs to deep tumor sites via a thermophoretic force [175].

Ultrasound. Ultrasound-activated theranostics are a combination of sonodynamic therapy [176], high-intensity focused ultrasound-induced thermal damage, and ultrasound-augmented imaging [177]. Additionally, ultrasound, particularly focused ultrasound, can be exploited to trigger drug release from the theranostic nanomedicine through an ultrasound-induced sonoporation effect or ultrasound-assisted microbubble destruction. An activatable Au-DNA nanoswitch was explored to realize ultrasound-triggered drug release. Double-stranded DNA as a mechanophore was bridged between two gold nanoparticles, and the resulting nanostructure was then loaded with DOX to obtain an ultrasound-activatable nanomedicine. As observed in the TEM images, the percentage of closed dimers significantly decreased, while single particles or aggregated particles steadily increased with an increase in the ultrasonication time. Besides, the open-dimer configuration appeared at 10 min post-ultrasonication and it was then reduced. These TEM images combined with rapid drug release from

the ultrasonication-treated Au-DNA nanoswitch unveiled drug release was induced from ultrasound-triggered force-stretched activation of the nanomedicine [178]. In another study, high-intensity focused ultrasound (HIFU) was employed to cleave 4,40-azobis (4-cyanovaleric acid) (ACVA) C-N bonds between the $\text{MnFe}_2\text{O}_4@ \text{CoFe}_2\text{O}_4$ core and the 1-adamantylamine- β -cyclodextrin cap to release the caged chemotherapeutic DOX. This de-capping release process was real-time monitored via enhanced MR contrast induced by an increased level of water around the magnetic nanoparticle core [87]. MR-guided focused ultrasound (MRgFUS) is currently used to treat mental disorders and it has shown promise in the application of cancer theranostics. The thermal effect induced by focused ultrasound can be employed to trigger controlled release of therapeutic drugs from the nanomedicine and offer thermal images of the tumor tissue. L-menthol as a thermal-sensitive valve, DOX, and Fe ions were incorporated into mesoporous organosilica nanoparticles as an ultrasound-induced thermal-activatable theranostic nanoagent. In this nanoagent, Fe-mediated T2WI revealed enhanced tumor accumulation of the nanotheranostic agent. MRgFUS induced a hyperthermia condition (45 °C) to open the L-menthol valve for robust DOX release [179].

To conclude, with the aid of sonosensitizers, low-energy ultrasound can be a preferable and safe choice for removing a cap or loosening a nanostructure to release incorporated drugs. In addition, the design of sonosensitizers is critical. For example, one recent study demonstrated that a protein coating on hydrophobic MSN nanoparticles could significantly increase the cavitation activity in contrast to coatings with F127 polymers or phospholipids [180].

Magnetic field. An exogenous circularly polarized magnetic field (MF) may act as an exogenous stimulus for ferrous metal-based nanoagents. A hybrid core-shell vesicle (HCSV), consisting of an ascorbic acid-containing core and an iron oxide nanocube-embedded PLGA shell, was reported to induce ferroptosis-like immune response-mediated cell death and activatable MRI under a MF. The MF destroyed the shell via a forced circular back-and-forth movement, and the released ascorbic acid in the core reacted with Fe_3O_4 to convert ferric to ferrous via the Fenton reaction. This was confirmed with a cube-like empty structure in the TEM images, a substantial increase in the absorbance of ferrous ions, a steady decline in the TRAMP-C1 tumor cell viability, and a significant increase in the CRT exposure (57.5 ± 2.7 %) after the TRAMP-C1 tumor cells were treated with HCSVs in a MF. An

activated MRI performance was supported with a significant reduction in the r_2 value of IONCs from 13.90 to 0.57 $\text{mM}^{-1}\text{s}^{-1}$ when incubated with ascorbic acid, and a remarkable boost in the T2 signal in the tumor area after *i.t.* injection of HCSVs in a MF compared to the injection without the MF. The therapeutic efficacy of HCSVs was raised with the aid of an exogenous MF. The average tumor weight of the TRAMP-C1-bearing mice treated with HCSVs reduced from 1.4 ± 0.3 g to 0.4 ± 0.3 g compared to 3.1 ± 0.2 g in the PBS-treated control group; the percentage of mature $\text{CD80}^+\text{CD86}^+$ DCs in lymph nodes increased from $27.9 \pm 0.9\%$ to $35.88 \pm 1.8\%$; the proportion of infiltrated CD8^+ T cells increased from $4.3 \pm 0.5\%$ to $7.7 \pm 0.8\%$ in the tumor area, and from $43.4 \pm 0.9\%$ to $46.2 \pm 1.9\%$ in lymph nodes (Figure 9) [181].

Overall, the magnetic field can manipulate ferrous metal agents and it may induce a magnetocaloric effect on some nanostructures. In this context, magnetic-driven forces and magnetic-induced temperature rises may be taken into consideration in the preparation of magnetic field-activated nanotheranostic agents.

3.2.6. Combined stimuli-activatable theranostic nanomedicine

In this section, we briefly present two typical combined activatable strategies: sequential activation by combined endogenous stimuli and combined activation by endogenous and exogenous stimuli.

Combined endogenous stimuli-mediated sequential activation. Based on the distinct location of endogenous stimuli, a stepwise dual/multiplexed activation strategy by endogenous stimuli has been explored. In a common paradigm, extracellular enzymes or tumor acidosis help induce charge reversal or size reduction of the nanomedicine to achieve its high cellular internalization and deep tumoral penetration, while the intracellular elevated level of redox or enzymes could trigger robust drug release or aggregation [182-184].

Enzyme plus redox. In one study, alkaline phosphatase (ALP) on tumor cell membranes was harnessed to induce dephosphorylation and self-assembly of an activatable fluorogenic small-molecule Pt(IV) prodrug, P-CyPt, for enhancing its cellular uptake; the dephosphorylation procedure resulted in a turn-on of the FL signal (710 nm) and the PA signal (700 nm); self-assembly of the prodrug enabled a turn-on of the PA signal at 750 nm. Furthermore, the intracellular GSH triggered the disassembly of the prodrug to release cisplatin and diminish the PA signal (750 nm). This dual stimuli-activatable strategy offered spatiotemporal tumor delineation and

drug-release monitoring, and it could hold great promise for precise cancer chemotheranostics (**Figure 10A**) [38]. In another study, apurinic/apyrimidinic endonuclease 1(APE1), an intracellular enzyme upregulated by an elevated redox level during ferroptosis, was employed as the second stimulus to a nanomedicine after GSH exposure. A GSH/APE1 cascade-activatable nanoassembly was developed to realize real-time monitoring of APE1 dynamics and APE1-mediated drug release. In this nanoassembly, ultrasmall iron oxide nanoparticles were functionalized with DNA, which was labelled with Cy5.5 and contained GSH-sensitive disulfide linkers. DNA-functionalized magnetic nanoparticles and DOX self-assembled into a stable nanoassembly. In this design, GSH exposure enabled the first-stage disassembly, leading to a switch from T2 to T1 MRI; APE1 facilitated the second-stage disassembly with recovery of fluorescence signal and DOX release [186].

pH plus redox. It was reported that H⁺ facilitated dissociation of zeolitic imidazolate framework-8 coating and then GSH induced aggregation of the core gold nanorods via Au-thiol and zwitterionic electrostatic interaction. This design in the nanomedicine enabled a shift of the excitation laser wavelength for PAI and PTT from NIR-I (810

nm) to NIR-II (1048 nm) in a combined endogenous stimuli-activated manner [187]. In another study, a pH/redox-responsive theranostic nanoprobe was developed with spatiotemporal dynamic fluorescence intensity conversion, and the nanoprobe was the self-assembly product of ICG and GSH-responsive dasatinib (DAS) dimers. In terms of imaging, the aggregation-induced emission (AIE) enhancement in tumor sites was achieved after accumulation of the theranostic nanoprobe, while intracellular pH/redox-induced disintegration of the nanoprobe led to the quenching of the AIE; the release of water-soluble ICG contributed to an enhancement in the fluorescence signal. This hypothesis was confirmed from *in vivo* fluorescence imaging of the K562-bearing mice: the FL intensity in the tumor tissues experienced its first drop at 4 h and then a steady increase in the following 20 h. For the therapeutic treatment, a high level of tumor accumulation of the nanomedicine and intracellular pH/redox-triggered DAS release contributed to a remarkable therapeutic efficacy compared to free DAS drugs on both K562 and H22 tumor-bearing mice (**Figure 10B**) [185]. In another study, Fe(III)-coordinated croconaine molecules were mixed with bovine serum albumin (BSA) to fabricate the

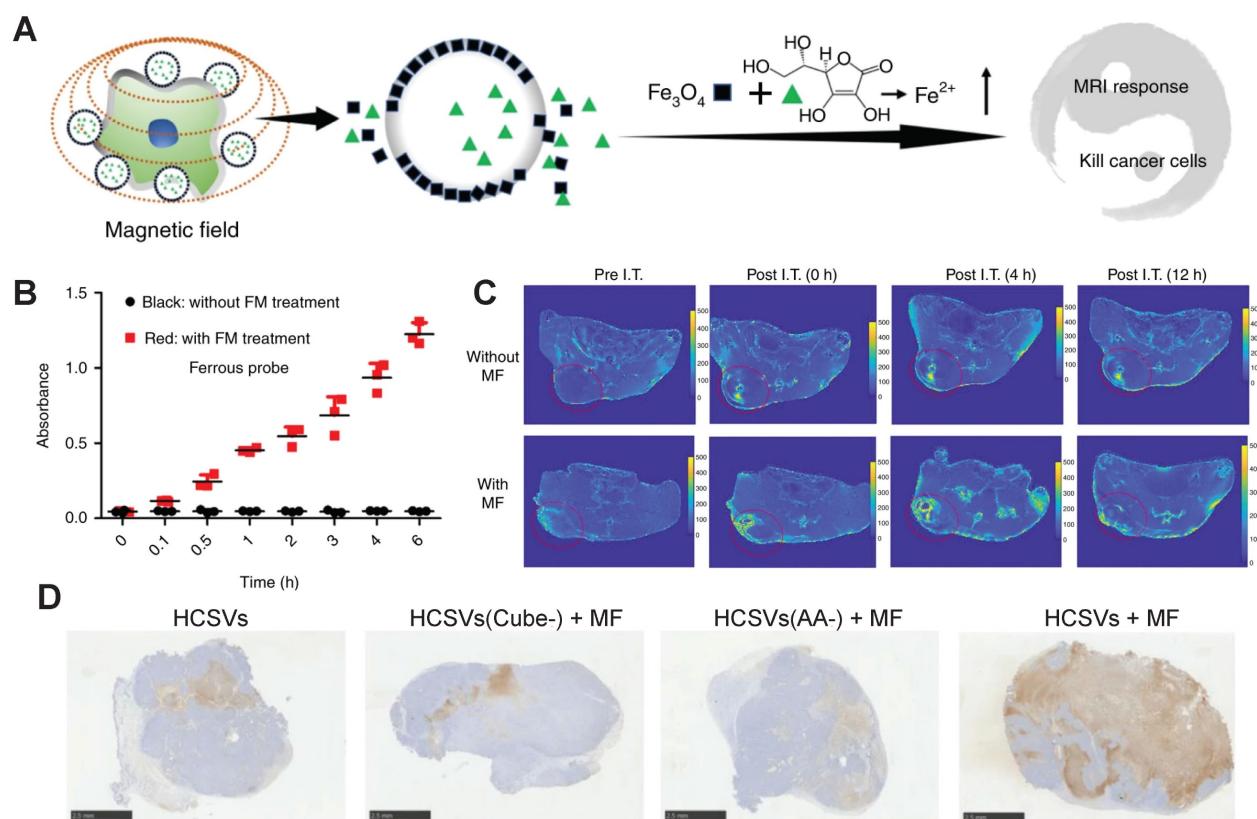


Figure 9. Magnetic field-activatable nanomedicine for cancer theranostics. Magnetic field-activatable hybrid core-shell vesicles for ferroptosis-like cell death-mediated immunotherapy and MRI. A) Schematic of the vesicles for MRI and therapy in a magnetic field. B) Change in the concentration of ferrous ions that were released from this vesicle with/without a FM at different time points. C) *In vivo* T2 mapping of the tumor site after *i.t.* injection of the nanovesicles with or without a magnetic field. D) TUNEL-stained tumor slices of the TRAMP-C1 model after different treatments, scale bar: 2.5 mm. Reproduced with permission [181]. Copyright 2020 the Authors, published by Springer Nature.

Cro-Fe@BSA nanomedicine that were sensitive to both pH and redox. The release rate of iron ions, the absorption rate of Cro-Fe@BSA, the generation rate of •OH radicals, the PA signal, and the r_1/r_2 ratio were improved as pH decreased. The reversible absorbance of the Cro-Fe complex indicated that GSH could facilitate the Fe^{3+} -to- Fe^{2+} conversion. This pH/redox dual stimuli-activatable strategy promoted a synergistic antitumor effect of ferroptosis and photothermal therapy. CLSM imaging of BIDIPY-stained treated cells revealed that the green fluorescent intensity (an indicator of lipid peroxidation formation) in Cro-Fe@BSA-treated cells was much stronger than that in the cells treated by the control, Cro@BSA, and Cro@BSA/laser. Notably, the green fluorescent intensity of the Cro-Fe@BSA-treated cells increased by 1.67-fold upon exposure to light irradiation and decreased by 5.1-fold after adding a ferroptosis inhibitor. These findings together with

regulated expression of GPX4 and HSP70 indicated that the generated photothermal effect aided in generation of •OH radicals and lipid peroxide. Moreover, the employment of Cro-Fe@BSA with the PA and MR imaging properties could help determine the optimal therapeutic window time (24 h) [188].

pH plus redox plus glucose. *In vivo* application of companion diagnostics was demonstrated with a glucose oxidase (GOx)-engineered polyaniline-based nanoplatform via a reversible TK linker (denoted as PANITGs). In this nanoplatform, pH-activatable polyaniline acted as a PTT agent and GOx in PANITGs reacted with glucose to generate H_2O_2 and glutamic acid. The wavelength of PANITGs redshifted under an acidic tumor environment. The PTT and PAI by the nanoplatform were amplified with a self-destructive effect induced by GOx catalysis-mediated breakage of a H_2O_2 -cleavable thioketal linker. The PA signal of the tumor area

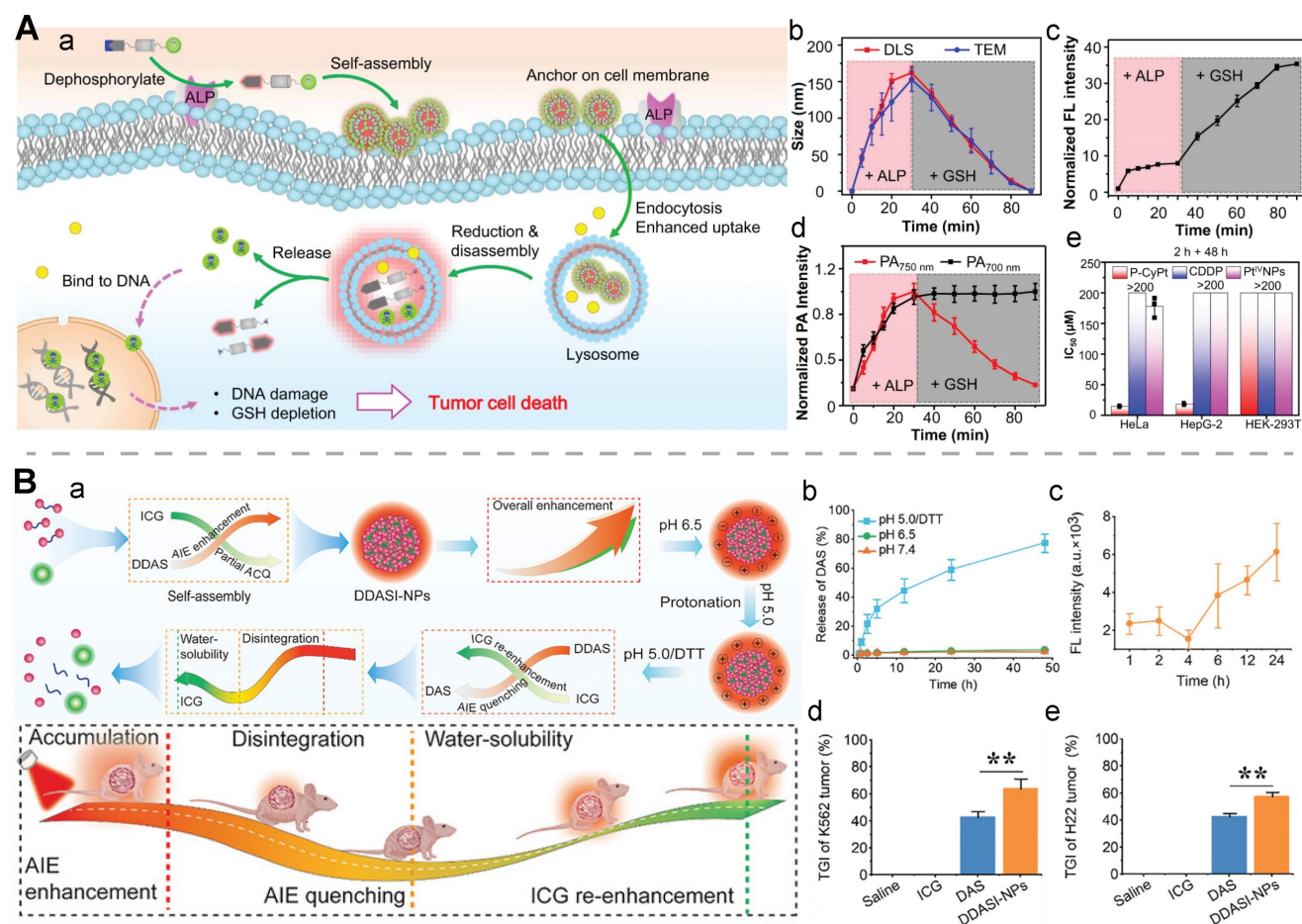


Figure 10. Dual endogenous stimuli-activatable nanomedicine for cancer theranostics. A) An enzyme/GSH-activatable fluorogenic cisplatin prodrug (P-CyPt) with extracellular self-assembly and intracellular disassembly for FL/PA imaging-guided chemotherapy of liver tumors. a) Schematic illustration of self-assembly and disassembly of the prodrug at different locations. b) Size, c) FL intensity, and d) PA intensity of this fluorogenic prodrug after sequential addition of alkaline phosphatase (ALP) and GSH. e) The IC_{50} values of the prodrug and its controls on tumor cells (HeLa and HepG-2) and normal cell (HEK-293T). Reproduced with permission [38]. Copyright 2021 the Authors, published by Springer Nature. B) A pH/GSH-activatable theranostic nanoprobe (DDASI-NPs) for FL imaging-mediated spatiotemporal monitoring of the chemotherapeutic outcome. a) Scheme of the proposed working principle of the nanoprobe. b) Release profile of DAS at different conditions. c) Semiquantitative analysis of *in vivo* fluorescence intensity in tumor sites injected with this theranostic nanoprobe. Tumor growth inhibition (TGI) in d) the K562 tumor-bearing mice and e) the H22 tumor-bearing mice after different treatments. Reproduced with permission [185]. Copyright 2023, Wiley-VCH.

reached a peak at 4 h post-injection of the polyaniline (PANI) nanostructure and PANITG with an SNR of 2.0 and 2.9, respectively, indicating their ability to image the tumoral microenvironment. PA images with multi-wavelengths confirmed that the hemoglobin–oxygen saturation percentage distinctly declined from 24.4% to 7.4% in the PANITG-treated mice, comparing with a negligible change in the percentage in the mice treated with PANI, revealing the GOx-assisted starvation therapeutic role of PANITG (**Figure 11**) [189].

Integrated endogenous stimuli with exogenous stimuli-mediated activation. Integration of a remote exogenous stimulus with endogenous stimuli has been recently considered for designing activatable theranostic nanomedicine for more precise tumor control [190].

Light + endogenous stimuli-induced activation. In the light-induced theranostic nanomedicine, light-exerted physical stress, nanostructure-enhanced ROS generation, and/or a temperature rise could be the activation effects for the nanomedicine. Light in combination with endogenous stimuli would expand the avenue of intelligent nanomedicine for cancer theranostics.

Light/redox activation. A self-sacrificed nanoassembly (NP@PE^{DOX}/PSP) self-assembled from a pseudo-semiconducting polymer (PSP) with a photo-theranostic property and DOX-conjugated amphiphilic polyester (PE^{DOX}). In this nanostructure, disulfide bonds were introduced in both PSP and PE^{DOX} for constructing biodegradable nanostructure and ROS-sensitive thioketal linkers at the DOX-conjugated site for realizing DOX release via ROS

stimulation indirectly generated by light. HPLC analysis revealed that NP@PE^{DOX}/PSP realized light-induced DOX release, while a negligible DOX amount was released without light irradiation. An increase in the elution time points of PSP and PE^{DOX} in the GPC chromatogram after incubation with GSH also supported the GSH-responsive degradability of this nanostructure. Notably, a continuous enhancement in the fluorescent intensity was seen at the tumor site in the first 24 h after *i.v.* injection of NP@PE^{DOX}/PSP, indicating a time point of 24 h could be appropriate for subsequent light irradiation. The therapeutic outcome of NP@PE^{DOX}/PSP through light-assisted combined therapy was confirmed with a significant tumor suppression effect and an enhancement in the percentage of infiltrated CD8⁺ T cells for up to 28.4% (**Figure 12A**) [191]. Another study explored the manipulation of the aggregation status of a nanomedicine through the intracellular redox stimuli to trigger potent NIR-II light absorption for PAI and PTT. In this design, self-assembled gold nanochains were encapsulated in mesoporous silica nanoparticles (AuNCs@SiO₂), and citrate ligands were coated on gold nanoparticles. The ligands were detached upon exposure to over-expressed H₂O₂ in the TME, contributing to a potent PCE of 82.2% via improved charge transfer between adjacent gold nanoparticles [192].

Light/pH activation. One recent study explored spatiotemporal control of metal-free tumor ferroptosis by a pH/light-activatable nanomedicine. This nanomedicine was prepared from phenothiazine-fused oxazine biotinylated nanoparticles (PTO-Biotin NPs), an oxazine-based photothermal molecular assembly.

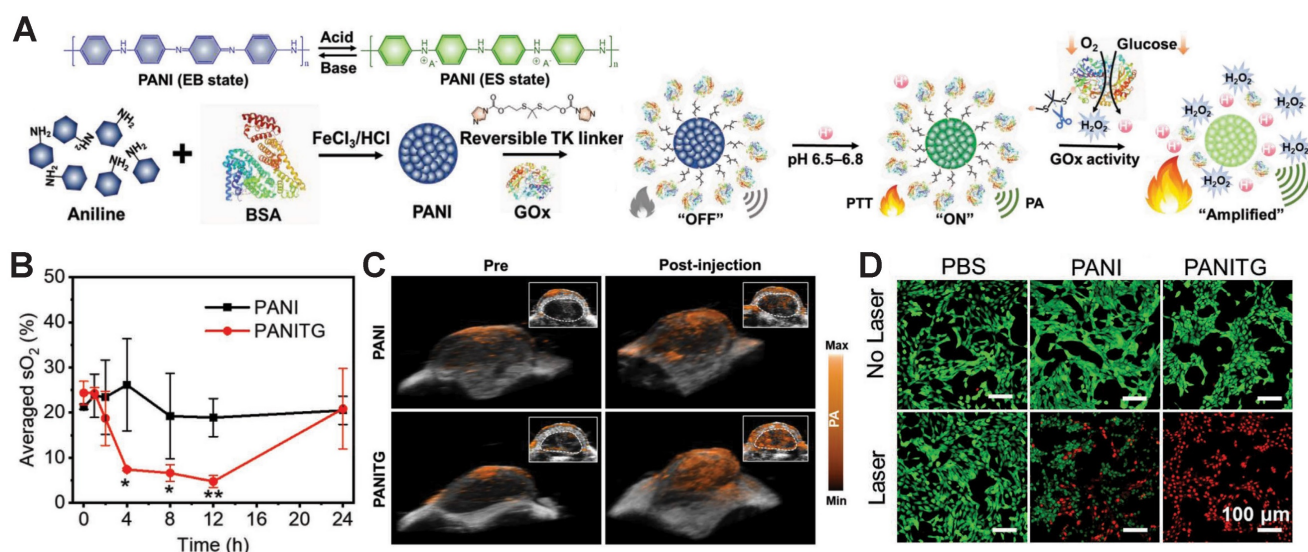


Figure 11. A pH/glucose/H₂O₂ triple-activatable conjugated polymeric nanoplatform (PANITG) for activatable photoacoustic imaging, photothermal therapy, and starvation therapy. A) Schematic of the activation mechanisms for imaging and therapy of PANITG. B) Quantification of the volume-averaged PA signal and the oxygen saturation (sO₂) level at the tumor site and C) 3D PA images of tumor sites treated with PANI and PANITG. D) Live-dead cells staining of 4T1 cells after different treatments. Reproduced with permission [189]. Copyright 2022, Wiley-VCH.

An acidic lysosomal environment activated the pH-responsive photothermal ingredient PTO₂, and NIR light activation enhanced lysosomal dysfunction through remarkable Fenton reaction-promoted ferroptosis [193]. In another study, the NIR light-generated thermal effect along with the tumor acidosis was employed to trigger intelligent release of chemotherapeutic DOX from PCN-DOX@PDA, a DOX-encapsulated and polydopamine (PDA)-coated PCN-600 nanoparticle. The chelated Fe ions in PCN-600 facilitated magnetic resonance imaging and the PDA coating shell enhanced the imaging performance with a 4-fold increase in the r_2 value (from 8.23 to 32.84 mM⁻¹ s⁻¹) [194]. A smart PDT/PTT complementary therapeutic strategy in response to light/pH/hypoxia-associated enzyme was proposed. In the extracellular environment of tumor cells, a low pH triggered the disassembly of BDP-Oxide NPs for the following fluorescence imaging-guided PDT. After these NPs deeply penetrated into tumor tissues, cytochrome P450 in these deep tumor sites featured with a low oxygen tension reduced BDP-Oxide into BDP, thus activating photoacoustic imaging-guided

PTT. As a result, this smart theranostic nanomedicine contributed to a high tumor inhibition rate of 94.8% on the HepG2 tumor-bearing nude mice [195].

Light/Enzyme activation. Aggregation of a nanomedicinal structure triggered by tumor-specific enzymes or other endogenous stimuli could enhance the photoactivation therapeutic efficiency. In one study, a SIA- α TSLs nanomedicine was obtained by encapsulating photosensitizers IR780, chemotherapeutic drugs abemaciclib, and magnetic Fe₃O₄ NPs in ACKFRGD-peptide and 2-cyano-6-amino-benzothiazole (CABT)-co-modified liposomes. In the presence of cathepsin B at the tumor site, the ACKFRGD peptide was cleaved to expose the 1,2-thiolamino groups of the AC peptide fragment, which would react with CABT via click cycloaddition to form nanoaggregates for enhanced near-infrared fluorescence imaging and MRI. Under this enhanced imaging guidance, the tumor sites were irradiated with NIR light. Thermal-enhanced drug release and thermal-induced damage resulted in a high tumor inhibition rate of 79.81 ± 5.30% (Figure 12B) [196].

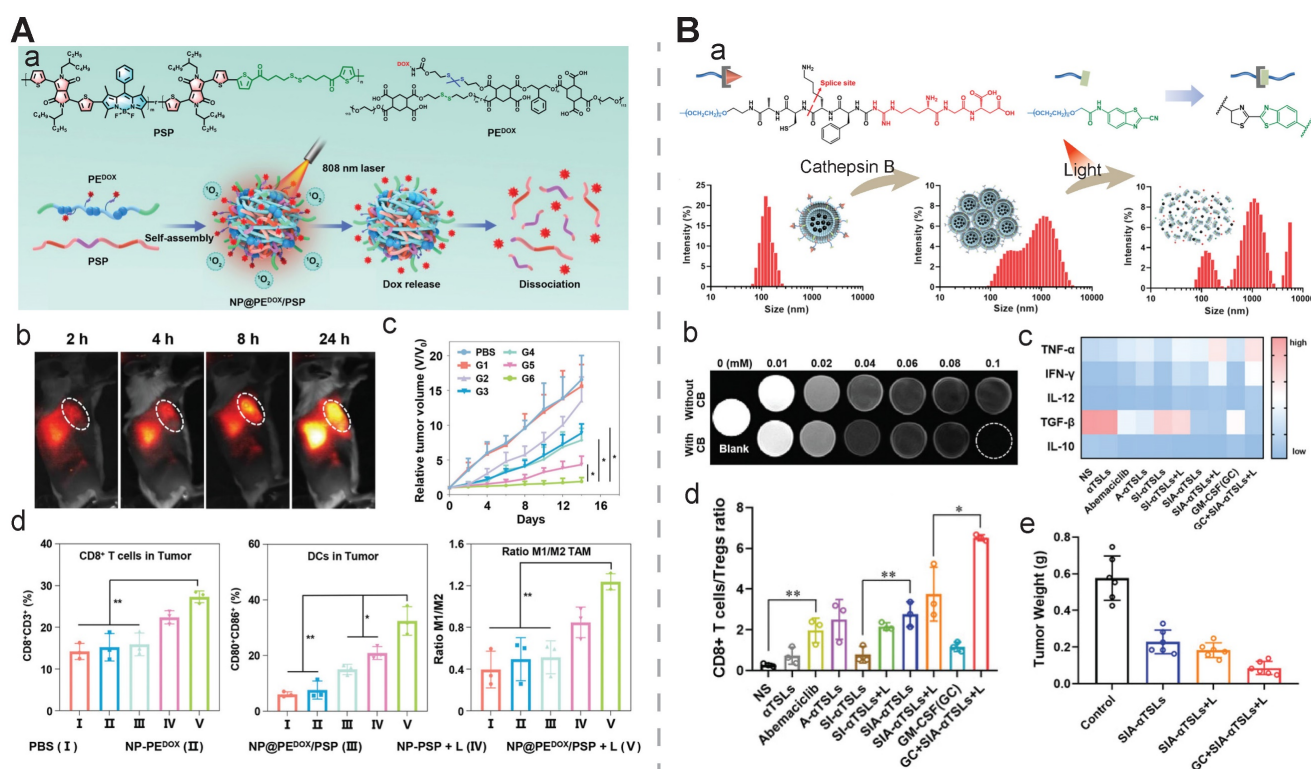


Figure 12. Combined exogenous/endogenous-activatable nanomedicine for cancer theranostics. **A**) Light/GSH-activatable pseudo-semiconducting polymeric nanoparticles (NP@PEDOX/PSP) for NIR-II fluorescence imaging, photodynamic immunotherapy, and photo-activated chemotherapy. **a**) Schematic of the preparation process of NP@PEDOX/PSP and its activation for imaging and therapy. **b**) *In vivo* NIR-II images of a murine tumor model treated with NP@PEDOX/PSP at different time points. **c**) Tumor growth curves of the mice groups treated with different methods, including PBS, NP-PSP (G1), DOX (G2), NP-PEDOX (G3), NP@PEDOX/PSP (G4), NP-PSP + L (G5), and NP@PEDOX/PSP + L (G6). **d**) Quantitative analysis of CD8⁺ T cells in the tumor site and the spleen, CD80⁺CD86⁺ DCs in the tumors, and the M1/M2 ratio in the tumors from different groups. Reproduced with permission [191]. Copyright 2022, Wiley-VCH. **B**) Light/enzyme-activatable SIA- α TSLs for MRI/NIRF-guided photothermal therapy. **a**) Changes in the chemical structure and hydrodynamic size via DLS of SIA- α TSLs after sequential activation by cathepsin B and light. **b**) T2WI of SIA- α TSLs incubated with/without cathepsin B. **c**) Intratumoral cytokines; **d**) ratios of CD8⁺ T cells to Tregs in the tumor tissue; and **e**) tumor weights at the endpoint of the CT26-bearing mice after different treatments. Reproduced with permission [196]. Copyright 2022 the Authors, published by Wiley-VCH.

Magnetic field + endogenous stimuli-induced activation. One common theranostic application of a magnetic field is to stimulate magnetic nanoparticles for magnetic hyperthermia therapy and T2WI magnetic resonance imaging. One recent study adopted the pH-activatable charge-reversible organic coating strategy on surface modification of magnetic nanoparticles for inducing their intracellular aggregation. Two pH-responsive nanosystems, A-M5&M20 and A-M20&M20, were prepared by integrating M20@DPA/HA with negatively charged magnetic nanoparticles with different sizes (M5 and M20). According to the TEM images, heating curves, and MR images of various samples (M5, M20, M20@DPA/HA, A-M5&M20 or A-M20&M20), pH-activatable aggregation formation resulted in with a size-dependent magneto-thermal conversion efficiency: the aggregates from A-M20&M20 displayed a 20-fold increase in the conversion efficiency compared to individual nanoparticle M5, and a more than two-fold increase in the size and the r_2 value compared to the single magnetic nanoparticle. After various treatments of the orthotopic 4T1-bearing mice under an AMF, the highest tumor inhibition rate of 83.8% was achieved in the A-M20&M20-treated group [197].

Ultrasound + endogenous stimuli-induced activation. Ultrasound often acts as an activation source for sonosensitizers and/or an initiator for the opening of cellular barriers, while various endogenous stimuli aid in disintegrating a nanomedicine to release therapeutic/imaging agents. In one recent study, an Mn-doped hollow MSN with a sonosensitizer Rose Bengal and a NO donor SNO was developed for ultrasound-triggered SDT and nitric oxide therapy. In this design, pH and GSH promoted Mn^{2+} release for an enhanced contrast of MRI: a ~3-fold increase in the r_1/r_2 value was seen after this nanomedicine was incubated in a TME-simulated buffer (pH 5.2, 5 mM GSH) compared to that in a normal environment-simulated one (pH 7.4). Meanwhile, an escalated increase in ROS generated by Rose Bengal and NO released by SNO contributed to the production of highly reactive ONOO \cdot for a synergistic antitumor effect; the average tumor size in the group treated with this combined therapy (MH-SNO@RB + US) was significantly reduced by ~82% [66].

Overall, these combined endogenous stimuli-activatable strategies can be generalized for designing theranostic nanomedicine with an outstanding imaging/therapeutic performance. The perturbation in the TME after the interventions of nanomedicine

with exogenous stimuli could be systematically profiled and endogenous stimuli could be identified to align with the perturbation in the TME to realize synergistic imaging or therapeutic effects.

4. Reflection and future perspectives

After an in-depth dive into the working principles, designs, recent advances, and current clinical status (Table 4) of stimuli-activatable nanomedicine for cancer theranostics, we provide a few reflections into this topic: a) A better understanding of tumor biology is essential for the optimization of stimuli-activatable nanomedicine, such as the altered concentrations of tumor biomarkers at different cancer types/stages and after different interventions; b) Insufficient stimulus-responsiveness of a nanomedicine may originate from an inadequate dose of endogenous stimuli or a relative low intensity of external stimulation, a weak response of activatable ligands in the nanomedicine to endogenous or exogenous stimuli or a poor efficiency in breaking them, or excessive consumption of endogenous stimuli (e.g., GSH); c) Novel and efficient stimuli-activatable linkers and nanostructures for the nanomedicine have been explored, while there lacks a systematic investigation into their breakage efficiencies towards their corresponding stimuli using a generalized nanopatform; d) An incorrect or incompatible fabrication method or an inappropriate synthetic route may lead to pre-cleavage of sensitive linkers or nanostructures in the nanomedicine; e) Exogenous stimuli can exert stimulation in both direct and indirect manners, which should be taken into consideration for the design of nanomedicine for cancer theranostics; f) The “all in one” strategy prevails in the nanomedicine design: functional agents are integrated into one single nanocarrier to realize multiple modalities of imaging/therapy or imaging-guided therapy, which could significantly deter the clinical translation of stimuli-activatable nanomedicine. Instead, one single agent with a well-established mechanism of action could be considered for integration into nanomedicine.

Based on these reflections, we propose the following future directions in the development of activatable nanomedicine for cancer theranostics:

i. The “activator-quencher” strategy for activatable theranostic nanoagents has been demonstrated with great potential in clinical application, and more pairing agents should be discovered for on-demand drug release or site-specific signal turn-on.

Table 4. Stimuli-activatable nanomedicine for cancer imaging/therapy in clinical trials or practices

| Stimuli | Activatable nanomedicine | Descriptions | Indications | Clinical status |
|----------------|----------------------------------|--|---|--|
| pH | ONM-100 | Micelle covalently conjugated to indocyanine green for imaging-guided surgery | Solid tumor; peritoneal metastases; lung malignancies | NCT03735680 (phase II, completed); NCT04950166 (phase II, recruiting); NCT05048082 (phase II, completed) |
| | NC-6300 | Polymer micelle with hydrazine-linked epirubicin | Advanced solid tumors or soft tissue sarcoma | NCT03168061 (phase I/II, unknown status) |
| | CRLX101 | Cyclodextrin-containing polymer with glycine-linked camptothecin | Advanced non-small cell lung cancer | NCT01380769 (phase II, completed) |
| Redox | Mirvetuximab soravtansine | FR α -targeted antibody conjugated to maytansinoid DM4 via disulfide linker | Ovarian cancer | Approved, 2022 |
| | Inotuzumab ozogamicin (Besponsa) | anti-CD22 conjugated to calicheamicin via disulfide and hydrazone linkers | Lymphoblastic leukemia | Approved, 2017 |
| | LS301 | A NIR fluorescent dye and an octapeptide that is cyclized through a disulfide bond | Breast cancer | NCT02807597 (phase I/II, recruiting) |
| Enzyme | Brentuximab vedotin (ADCETRIS®) | AntiCD30 conjugated to MMAE via cathepsin B-cleavable linkers | lymphoma | Approved, 2011/2012 |
| | Paclitaxel polyglumex (Opaxio™) | Paclitaxel polymeric NPs sensitive to cathepsin B | Head and neck cancer; glioblastoma | Approved, 2012 |
| | LiPlaCis | Liposomal formulated cisplatin sensitive to phospholipase A2 | Advanced or refractory tumors | NCT01861496 (phase I/II, completed) |
| | CX-072 | Anti-PD-L1 based on activatable Probody™ | Solid tumor; lymphoma | NCT03013491 (Phase I/II, completed) |
| Hypoxia | 18F-FMISO | Activatable PET probe | Anaplastic glioma | NCT01200134 (phase II, completed) |
| | [18F]HX4 | Activatable PET probe | Head and neck and lung cancer | NCT02976883 (phase II, completed) |
| | ¹⁸ F-EF5 | Activatable PET probe | Non-small cell lung cancer | NCT01017133 (phase I, completed) |
| Temperature | ThermoDox® | Thermosensitive liposome containing doxorubicin | Hepatocellular carcinoma | NCT02112656 (phase III, completed) |
| Radiation | CriPec® docetaxel | Thermosensitive polymeric micelles containing docetaxel | Solid tumors | NCT02442531 (phase I, completed) |
| | NBTRX3 | Hafnium oxide NPs for CT and radiosensitization | LA-HNSCC; Locally advanced soft tissue sarcoma | NCT04892173 (phase III, completed); European market approval, 2019 |
| | AGuIX | Polysiloxane Gd-chelates based nanoparticles for MRI and radiosensitization | Multiple brain metastases | NCT03818386 (phase II, recruiting) |
| Magnetic field | NanoTherm® | Amino silane-coated Fe ₃ O ₄ nanoparticles for MRI and MHT | Glioblastoma | Approved by EMA, 2010 |
| | Magnetic nanoparticles | Magnetic thermoablation | Prostate cancer | Completed, NCT02033447 (early phase I, completed) |
| Light | AuroLase® (AuroShell) | PEG-coated silica gold nanoshells for NIR-activated thermoablation | Head and neck cancer | NCT00848042 (not applicable, completed) |
| | Photobac® | 3-(1-Butyloxy)ethyl-3-deacetyl-bacterioporpurin-18-n-butylimide methyl ester for intracavitary PDT | Glioblastoma or gliosarcoma | NCT05363826 (phase I, recruiting) |
| Ultrasound | Melanin | An endogenous light-absorber | Melanoma | NCT02613325 (phase I, completed) |
| | Sonazoid | Perfluorobutane gas-containing MB | Focal liver lesions | Approved (2007 in Japan and 2019 by NMPA of China) |
| | Microbubbles | US-triggered MB destruction for sonoporation | Colorectal cancer hepatic metastases | NCT03458975 (phase II, completed) |
| | Optison™ | Perflutren protein-type A microspheres for US and US-triggered MB destruction | Hepatocellular Carcinoma | NCT03199274 (phase II, recruiting) |

FR α : folate receptor α ; MMAE: monomethyl auristatin E; FMISO: fluoromisonidazole; LA-HNSCC: locally advanced head and neck squamous cell carcinoma; EMA: European Medicines Agency; MHT: magnetic hyperthermia therapy; NIR: near-infrared light; MB: microbubble; NMPA: national medical products administration.

ii. Tumor enzyme-activatable strategy may become predominant in the nanomedicine for cancer theranostics since other endogenous stimuli may not be tumor-specific during the treatment of cancer patients with other accompanying diseases.

iii. In-situ synthesis of theranostic nanoagents with an aggregation-enhanced performance is encouraging. For instance, co-injection of CBT-NOTA-⁶⁸Ga and CBT-NOTA-Ga led to their self-assembly into NPs after exposure to a high level of furin, and these NPs displayed enhanced microPET imaging contrast at a reduced dose of the imaging radioisotope [43]. Similarly, the stimuli-triggered self-assembly of theranostic radioisotopes may escalate their therapeutic effects.

iv. To address insufficient stimuli-responsiveness, supply of extra endogenous stimulus agents via nanocarriers could be considered to improve the diagnosis/therapeutic efficiency of the corresponding activatable theranostic nanomedicine. In addition, activatable ligands that efficiently respond to stimuli and stimuli-cleavable chemistry should be explored.

v. With biological processes unveiled after therapeutic treatment, more specific or over-expressed stimuli can be exploited to construct an activatable nanomedicine to predict its therapeutic response, enable early stratification, and realize synergistic effects.

vi. Effective generalized masking shields of the nanomedicine with a stimuli-induced detachment behavior should be promoted as they can reduce the toxicity of therapeutic/imaging agents in the nanomedicine and the nanomedicine could gain an accelerated clinical translation. Specific nanoengineering of the masking shields in the nanomedicine could be advantageous for some unique, advanced cancer types.

vii. Nanorobotics that are driven by external stimuli or local stimuli could arrive at the target site with a high penetration ability to achieve great accumulation. Nanorobotic components could be integrated into the nanomedicine for cancer theranostics.

viii. Advanced tools, such as omics (radiomics, proteomics, and metabolomics) and artificial intelligence could be embraced to optimize the nanomedicine design based on large-scale data analysis [198, 199].

5. Conclusions

Nanoengineering the structure of medicine for cancer theranostics has thrived in the last two decades, and the stimuli-activatable strategy is one of the most promising engineering methods. The use of endogenous or exogenous stimuli for developing stimuli-activatable nanomedicine improves the specificity of on-site imaging or theranostics in addition to a high level of nanostructures-mediated tumor accumulation and mitigated toxicity to normal tissues. With the efforts of experts in multiple disciplines, simple but effective nanomedicine with a distinct mechanism of stimuli-activatable synergistic action will be translated into clinical application and benefit cancer patients.

Abbreviations

AI-Egen: aggregation-induced emission luminogens; APC: antigen-presenting cell; ATP: adenosine-5'-triphosphate; BODIPY: boron dipyrromethene; CDT: chemodynamic therapy; CLI: Cherenkov luminescence imaging; CMC: chemistry, manufacture and control; CRIC: Cherenkov radiation-induced cancer therapy; CT: computed tomography; EPR: enhanced permeability and retention; FRET: fluorescence resonance energy transfer; GGT: gamma-glutamyl transpeptidase; GSH: glutathione; HIFU: high-intensity focused ultrasound; MF: magnetic field; MMP: matrix metalloproteinases; MRI: magnetic resonance imaging; MRgFUS: MR-guided focused ultrasound; PAI: photoacoustic imaging; PANI: polyaniline; PCE: photothermal conversion efficiency; PDMAEMA: poly (*N,N*-dimethylaminoethyl methacrylate); PDT: photodynamic

therapy; PET: positron emission tomography; PROTACs: PROteolysis Targeting Chimeras; PTT: photothermal therapy; QDs: quantum dots; ROS: reactive oxygen species; RT: radiation therapy; SCAN: sonoafterglow cancer nanoimmunotheranostic probe; SDT: sonodynamic therapy; SEC: size-exclusion chromatography; SI: signal intensity; SNR: signal-to-noise ratio; TADF: activate thermally activated fluorescence; TMEP: 2,2,6,6-tetramethylpiperidine; TEMPO: 2,2,6,6-tetramethylpiperidine 1-oxyl; TME: tumor microenvironment; TSLs: thermosensitive liposomes; US: ultrasound; USPIO: ultrasmall superparamagnetic iron oxide.

Acknowledgements

Graphic Abstract, Figure 1-3, and Figure 6B were created with BioRender.com. This work was financially supported by the National Natural Science Foundation of China (52073193, 51873120, 81621003, 82202310), 1 3 5 project for disciplines of excellence, West China Hospital, Sichuan University (ZYJC21013).

Author Contributions

H.-N. Li, Y. Feng, and K. Luo conceived the outline of this review. H.-N. Li and Y. Feng collected papers for writing. H.-N. Li drafted the original manuscript and performed the creation of figures/tables. Y. Feng and Q. Luo helped create figures/table. Z.-Q. Li, X. L., H.-T. Gan, Z.-W. Gu, and Q.-Y. G helped revise the manuscript and discuss the content. K. Luo supervised this project and finalized this manuscript. All authors have read and approved the final manuscript.

Competing Interests

The authors have declared that no competing interest exists.

References

- Bhatia SN, Chen X, Dobrovolskaia MA, Lammers T. Cancer nanomedicine. *Nat Rev Cancer*. 2022; 22: 550-6.
- Gawne PJ, Ferreira M, Papaluca M, Grimm J, Decuzzi P. New opportunities and old challenges in the clinical translation of nanotheranostics. *Nat Rev Mater*, in press. doi: 10.1038/s41578-023-00581-x.
- Zeng F, Nijjati S, Liu Y, Yang Q, Liu X, Zhang Q, et al. Ferroptosis MRI for early detection of anticancer drug-induced acute cardiac/kidney injuries. *Sci Adv*. 2023; 9: eadd8539.
- Li H, Luo Q, Zhang H, Ma X, Gu Z, Gong Q, et al. Nanomedicine embraces cancer radio-immunotherapy: mechanism, design, recent advances, and clinical translation. *Chem Soc Rev*. 2023; 52: 47-96.
- Xu D, Ge J, An Y, Bai S, Wang Z, Wu S, et al. Molecular engineering of NIR-II/III emitting AI-Egen for multimodal imaging-guided photo-immunotherapy. *Small*. 2023; 19: 2300859.
- Xiao X, Cai H, Huang Q, Wang B, Wang X, Luo Q, et al. Polymeric dual-modal imaging nanoprobe with two-photon aggregation-induced emission for fluorescence imaging and gadolinium-chelation for magnetic resonance imaging. *Bioact Mater*. 2023; 19: 538-49.
- Luo K, Liu G, Zhang X, She W, He B, Nie Y, et al. Functional L-lysine dendritic macromolecules as liver-imaging probes. *Macromol Biosci*. 2009; 9: 1227-36.
- Mi P. Stimuli-responsive nanocarriers for drug delivery, tumor imaging, therapy and theranostics. *Theranostics*. 2020; 10: 4557-88.

9. Chagri S, Ng DYW, Weil T. Designing bioresponsive nanomaterials for intracellular self-assembly. *Nat Rev Chem*. 2022; 6: 320-38.
10. Wang C, Wang Z, Chen S, Cui P, Qiu L, Zhou S, et al. Modulation of aggregation-caused quenching to aggregation-induced emission: finding a biocompatible polymeric theranostics platform for cancer therapy. *Macromol Rapid Commun*. 2021; 42: 2100264.
11. Voskuil FJ, Steinkamp PJ, Zhao T, van der Vegt B, Koller M, Doff JJ, et al. Exploiting metabolic acidosis in solid cancers using a tumor-agnostic pH-activatable nanoprobe for fluorescence-guided surgery. *Nat Commun*. 2020; 11: 3257.
12. Pallares RM, Mottaghy FM, Schulz V, Kiessling F, Lammers T. Nanoparticle diagnostics and theranostics in the clinic. *J Nucl Med*. 2022; 63: 1802-8.
13. Zhou J, Rao L, Yu G, Cook TR, Chen X, Huang F. Supramolecular cancer nanotheranostics. *Chem Soc Rev*. 2021; 50: 2839-91.
14. Zhu R, Jiang W, Pu Y, Luo K, Wu Y, He B, et al. Functionalization of magnetic nanoparticles with peptide dendrimers. *J Mater Chem*. 2011; 21: 5464-74.
15. Ding Y, Sun Z, Gao Y, Zhang S, Yang C, Qian Z, et al. Plasmon-driven catalytic chemotherapy augments cancer immunotherapy through induction of immunogenic cell death and blockage of IDO pathway. *Adv Mater*. 2021; 33: 2102188.
16. Kim D, Byun J, Kim SI, Chung HH, Kim YW, Shim G, et al. DNA-cloaked nanoparticles for tumor microenvironment-responsive activation. *J Control Release*. 2022; 350: 448-59.
17. Zhang D, He J, Zhou M. Radiation-assisted strategies provide new perspectives to improve the nanoparticle delivery to tumor. *Adv Drug Deliv Rev*. 2022; 193: 114642.
18. Gu L, Duan Z, Chen X, Li X, Luo Q, Bhamra A, et al. A transformable amphiphilic and block polymer-dendron conjugate for enhanced tumor penetration and retention with cellular homeostasis perturbation via membrane flow. *Adv Mater*. 2022; 34: 2200048.
19. Gu L, Duan Z, Li X, Li X, Li Y, Li X, et al. Enzyme-triggered deep tumor penetration of a dual-drug nanomedicine enables an enhanced cancer combination therapy. *Bioact Mater*. 2023; 26: 102-15.
20. Xu J, Song M, Fang Z, Zheng L, Huang X, Liu K. Applications and challenges of ultra-small particle size nanoparticles in tumor therapy. *J Control Release*. 2023; 353: 699-712.
21. Roy S, Bag N, Bardhan S, Hasan I, Guo B. Recent progress in NIR-II fluorescence imaging-guided drug delivery for cancer theranostics. *Adv Drug Deliv Rev*. 2023; 197: 114821.
22. Chen B, Liu L, Yue R, Dong Z, Lu C, Zhang C, et al. Stimuli-responsive switchable MRI nanoprobe for tumor theranostics. *Nano Today*. 2023; 51: 101931.
23. Zhou Z, Deng H, Yang W, Wang Z, Lin L, Munasinghe J, et al. Early stratification of radiotherapy response by activatable inflammation magnetic resonance imaging. *Nat Commun*. 2020; 11: 3032.
24. Wang C, Sun W, Zhang J, Zhang J, Guo Q, Zhou X, et al. An electric-field-responsive paramagnetic contrast agent enhances the visualization of epileptic foci in mouse models of drug-resistant epilepsy. *Nat Biomed Eng*. 2021; 5: 278-89.
25. Wang Z, Xue X, Lu H, He Y, Lu Z, Chen Z, et al. Two-way magnetic resonance tuning and enhanced subtraction imaging for non-invasive and quantitative biological imaging. *Nat Nanotechnol*. 2020; 15: 482-90.
26. Yan Y, Chen B, Yin Q, Wang Z, Yang Y, Wan F, et al. Dissecting extracellular and intracellular distribution of nanoparticles and their contribution to therapeutic response by monochromatic ratiometric imaging. *Nat Commun*. 2022; 13: 2004.
27. Fu Q, Feng H, Su L, Zhang X, Liu L, Fu F, et al. An activatable hybrid organic-inorganic nanocomposite as early evaluation system of therapy effect. *Angew Chem Int Ed Engl*. 2022; 61: 202112237.
28. Guo C, Sun L, Cai H, Duan Z, Zhang S, Gong Q, et al. Gadolinium-labeled biodegradable dendron-hyaluronic acid hybrid and its subsequent application as a safe and efficient magnetic resonance imaging contrast agent. *ACS Appl Mater Interfaces*. 2017; 9: 23508-19.
29. Duangjai A, Luo K, Zhou Y, Yang J, Kopeček J. Combination cytotoxicity of backbone degradable HPMA copolymer gemcitabine and platinum conjugates toward human ovarian carcinoma cells. *Eur J Pharm Biopharm*. 2014; 87: 187-96.
30. Cheng P, Pu K. Molecular imaging and disease theranostics with renal-clearable optical agents. *Nat Rev Mater*. 2021; 6: 1095-113.
31. Webb BA, Chimenti M, Jacobson MP, Barber DL. Dysregulated pH: a perfect storm for cancer progression. *Nat Rev Cancer*. 2011; 11: 671-7.
32. Cao F, Jin L, Gao Y, Ding Y, Wen H, Qian Z, et al. Artificial-enzymes-armed *Bifidobacterium longum* probiotics for alleviating intestinal inflammation and microbiota dysbiosis. *Nat Nanotechnol*. 2023; 18: 617-27.
33. Jin L, Cao F, Gao Y, Zhang C, Qian Z, Zhang J, et al. Microenvironment-activated nanozyme-armed bacteriophages efficiently combat bacterial infection. *Adv Mater*. 2023; 35: 2301349.
34. Cheung EC, Voudsen KH. The role of ROS in tumour development and progression. *Nat Rev Cancer*. 2022; 22: 280-97.
35. Zhang J, Gao B, Ye B, Sun Z, Qian Z, Yu L, et al. Mitochondrial-targeted delivery of polyphenol-mediated oxidases complexes against pyroptosis and inflammatory diseases. *Adv Mater*. 2023; 35: 2208571.
36. Niu B, Liao K, Zhou Y, Wen T, Quan G, Pan X, et al. Application of glutathione depletion in cancer therapy: enhanced ROS-based therapy, ferroptosis, and chemotherapy. *Biomaterials*. 2021; 277: 121110.
37. Valkenburg KC, de Groot AE, Pienta KJ. Targeting the tumour stroma to improve cancer therapy. *Nat Rev Clin Oncol*. 2018; 15: 366-81.
38. Wen X, Zhang R, Hu Y, Wu L, Bai H, Song D, et al. Controlled sequential in situ self-assembly and disassembly of a fluorogenic cisplatin prodrug for cancer theranostics. *Nat Commun*. 2023; 14: 800.
39. Sun M, Jiang H, Liu T, Tan X, Jiang Q, Sun B, et al. Structurally defined tandem-responsive nanoassemblies composed of dipeptide-based photosensitive derivatives and hypoxia-activated camptothecin prodrugs against primary and metastatic breast tumors. *Acta Pharm Sin B*. 2022; 12: 952-66.
40. Tan P, Cai H, Wei Q, Tang X, Zhang Q, Kopytynski M, et al. Enhanced chemo-photodynamic therapy of an enzyme-responsive prodrug in bladder cancer patient-derived xenograft models. *Biomaterials*. 2021; 277: 121061.
41. Roemhild K, Besse HC, Wang B, Peña Q, Sun Q, Omata D, et al. Ultrasound-directed enzyme-prodrug therapy (UDEPT) using self-immolative doxorubicin derivatives. *Theranostics*. 2022; 12: 4791-801.
42. Jin Q, Wu J, Wu Y, Li H, Finel M, Wang D, et al. Optical substrates for drug-metabolizing enzymes: recent advances and future perspectives. *Acta Pharm Sin B*. 2022; 12: 1068-99.
43. Chen P, Wang H, Wu H, Zou P, Wang C, Liu X, et al. Intracellular synthesis of hybrid gallium-68 nanoparticle enhances microPET tumor imaging. *Anal Chem*. 2021; 93: 6329-34.
44. Cheng X, Xia T, Zhan W, Xu HD, Jiang J, Liu X, et al. Enzymatic nanosphere-to-nanofiber transition and autophagy inducer release promote tumor chemotherapy. *Adv Healthc Mater*. 2021; 11: 2201916.
45. Bai H, Wang H, Zhou Z, Piao Y, Liu X, Tang J, et al. Histone deacetylase-triggered self-immolative peptide-cytotoxins for cancer-selective drug delivery. *Adv Funct Mater*. 2023; 33: 2214025.
46. Yang X, Tang Q, Jiang Y, Zhang W, Wang M, Mao L. Nanoscale ATP-responsive zeolitic imidazole framework-90 as a general platform for cytosolic protein delivery and genome editing. *J Am Chem Soc*. 2019; 141: 3782-6.
47. Hay N. Reprogramming glucose metabolism in cancer: can it be exploited for cancer therapy? *Nat Rev Cancer*. 2016; 16: 635-49.
48. Fu LH, Qi C, Lin J, Huang P. Catalytic chemistry of glucose oxidase in cancer diagnosis and treatment. *Chem Soc Rev*. 2018; 47: 6454-72.
49. Singleton DC, Macann A, Wilson WR. Therapeutic targeting of the hypoxic tumour microenvironment. *Nat Rev Clin Oncol*. 2021; 18: 751-72.
50. Zhou R, Ohulchanskyy TY, Xu Y, Ziniuk R, Xu H, Liu L, et al. Tumor-microenvironment-activated NIR-II nanotheranostic platform for precise diagnosis and treatment of colon cancer. *ACS Appl Mater Interfaces*. 2022; 14: 23206-18.
51. Rathnamalala CSL, Hernandez S, Lucero MY, Swartzchick CB, Kalam Shaik A, Hammer NI, et al. Xanthene-based nitric oxide-responsive nanosensor for photoacoustic imaging in the SWIR window. *Angew Chem Int Ed Engl*. 2023; 62: 202214855.
52. Bai S, Lan Y, Fu S, Cheng H, Lu Z, Liu G. Connecting calcium-based nanomaterials and cancer: from diagnosis to therapy. *Nanomicro Lett*. 2022; 14: 145.
53. Sun H, Wang T, Ma W, Huang J, Chen B, Cheng H, et al. A stable DNA tetrahedra-AuNCs nanohybrid: on-site programmed disassembly for tumor imaging and combination therapy. *Biomaterials*. 2022; 288: 121738.
54. Zhang X, Li S, Ma H, Wang H, Zhang R, Zhang XD. Activatable NIR-II organic fluorescent probes for bioimaging. *Theranostics*. 2022; 12: 3345-71.
55. Ding Y, Tong Z, Jin L, Ye B, Zhou J, Sun Z, et al. An NIR discrete metallacycle constructed from perylene bisimide and tetraphenylethylene fluorophores for imaging-guided cancer radio-chemotherapy. *Adv Mater*. 2022; 34: 106388.
56. Qin Y, Geng X, Sun Y, Zhao Y, Chai W, Wang X, et al. Ultrasound nanotheranostics: toward precision medicine. *J Control Release*. 2023; 353: 105-24.
57. Geng J, Zhang Y, Gao Q, Neumann K, Dong H, Porter H, et al. Switching on prodrugs using radiotherapy. *Nat Chem*. 2021; 13: 805-10.
58. Choi H, Choi B, Han JH, Shin HE, Park W, Kim DH. Reactive oxygen species responsive cleavable hierarchical metallic supra-nanostructure. *Small*. 2022; 18: 2202694.
59. Guo Z, Hong H, Zheng Y, Wang Z, Ding Z, Fu Q, et al. Radiotherapy-induced cleavage of quaternary ammonium groups activates prodrugs in tumors. *Angew Chem Int Ed Engl*. 2022; 61: 202205014.
60. Liu N, Su X, Sun X. Cerenkov radiation-activated probes for deep cancer theranostics: a review. *Theranostics*. 2022; 12: 7404-19.
61. Soares PIP, Romão J, Matos R, Silva JC, Borges JP. Design and engineering of magneto-responsive devices for cancer theranostics: nano to macro perspective. *Prog Mater Sci*. 2021; 116: 100742.
62. Kubelick KP, Mehrmohammadi M. Magnetic particles in motion: magneto-motive imaging and sensing. *Theranostics*. 2022; 12: 1783-99.
63. Fan H, Guo Z. Tumor microenvironment-responsive manganese-based nanomaterials for cancer treatment. *Coord Chem Rev*. 2023; 480: 215027.
64. Torres-Herrero B, Armenia I, Alleva I, Asín L, Correa S, Ortiz C, et al. Remote activation of enzyme nanohybrids for cancer prodrug therapy controlled by magnetic heating. *ACS Nano*. 2023; 17: 12358-73.
65. Yang G, Liu Y, Chen J, Ding J, Chen X. Self-adaptive nanomaterials for rational drug delivery in cancer therapy. *Acc Mater Res*. 2022; 3: 1232-47.
66. Wang L, Tian Y, Lai K, Liu Y, Liu Y, Mou J, et al. An ultrasound-triggered nanoplatfor for synergistic sonodynamic-nitric oxide therapy. *ACS Biomater Sci Eng*. 2023; 9: 797-808.

67. Zhao Z, Dong S, Liu Y, Wang J, Ba L, Zhang C, et al. Tumor microenvironment-activable manganese-boosted catalytic immunotherapy combined with PD-1 checkpoint blockade. *ACS Nano*. 2022; 16: 20400-18.
68. Li X, Li W, Li K, Chen X, Wang C, Qiao M, et al. Albumin-coated pH-responsive dimeric prodrug-based nano-assemblies with high biofilm eradication capacity. *Biomater Sci*. 2023; 11: 1031-41.
69. Li J, Zhang X, Zhao M, Wu L, Luo K, Pu Y, et al. Tumor-pH-sensitive PLLA-based microsphere with acid cleavable acetal bonds on the backbone for efficient localized chemotherapy. *Biomacromolecules*. 2018; 19: 3140-8.
70. Liu H, Hu Z, Chen H, Yan Y, Le Z, Wei C, et al. Self-degradable poly(β -amino ester)s promote endosomal escape of antigen and agonist. *J Control Release*. 2022; 345: 91-100.
71. Guo S, Xiao X, Wang X, Luo Q, Zhu H, Zhang H, et al. Reductive microenvironment responsive gadolinium-based polymers as potential safe MRI contrast agents. *Biomater Sci*. 2019; 7: 1919-32.
72. Wan SC, Ye MJ, Yang QC, Zhang T, Zhang MJ, Ma XB, et al. Diselenide-based dual-responsive prodrug as pyroptosis inducer potentiates cancer immunotherapy. *Adv Healthc Mater*. 2023; 12: 2202135.
73. Li J, Luo Y, Zeng Z, Cui D, Huang J, Xu C, et al. Precision cancer sono-immunotherapy using deep-tissue activatable semiconducting polymer immunomodulatory nanoparticles. *Nat Commun*. 2022; 13: 4032.
74. Li Y, Qin Y, Shang Y, Li Y, Liu F, Luo J, et al. Mechano-responsive leapfrog micelles enable interactive apoptotic and ferroptotic cancer therapy. *Adv Funct Mater*. 2022; 32: 2112000.
75. Kim YE, Kim J. ROS-scavenging therapeutic hydrogels for modulation of the inflammatory response. *ACS Appl Mater Interfaces*. 2022; 14: 23002-21.
76. Zhang Y, Han X, Nie G. Responsive and activable nanomedicines for remodeling the tumor microenvironment. *Nat Protoc*. 2021; 16: 405-30.
77. Cai H, Tan P, Chen X, Kopytynski M, Pan D, Zheng X, et al. Stimuli-sensitive linear-dendritic block copolymer-drug prodrug as a nanopatform for tumor combination therapy. *Adv Mater*. 2022; 34: 2108049.
78. Zhou Q, Shao S, Wang J, Xu C, Xiang J, Piao Y, et al. Enzyme-activatable polymer-drug conjugate augments tumour penetration and treatment efficacy. *Nat Nanotechnol*. 2019; 14: 799-809.
79. Shi J, Wang Z, Shen C, Pan T, Xie L, Xie M, et al. Hypoxia degradable AIE photosensitizer with high efficiency of photodynamic therapy and improved biological safety. *Dyes Pigm*. 2022; 200: 110122.
80. Hou X, Chang YX, Yue YX, Wang ZH, Ding F, Li ZH, et al. Supramolecular radiosensitizer based on hypoxia-responsive macrocycle. *Adv Sci (Weinhl)*. 2022; 9: 2104349.
81. Liu J, Ai X, Cabral H, Liu J, Huang Y, Mi P. Tumor hypoxia-activated combinatorial nanomedicine triggers systemic antitumor immunity to effectively eradicate advanced breast cancer. *Biomaterials*. 2021; 273: 120847.
82. Rebelo C, Reis T, Guedes J, Saraiva C, Rodrigues AF, Simões S, et al. Efficient spatially targeted gene editing using a near-infrared activatable protein-conjugated nanoparticle for brain applications. *Nat Commun*. 2022; 13: 4135.
83. Tsai MF, Lo YL, Soorni Y, Su CH, Sivasoorian SS, Yang JY, et al. Near-infrared light-triggered drug release from ultraviolet- and redox-responsive polymersome encapsulated with core-shell upconversion nanoparticles for cancer therapy. *ACS Appl Bio Mater*. 2021; 4: 3264-75.
84. Gulfam M, Jo SH, Vu TT, Ali I, Rizwan A, Joo SB, et al. NIR-degradable and biocompatible hydrogels derived from hyaluronic acid and coumarin for drug delivery and bio-imaging. *Carbohydr Polym*. 2023; 303: 120457.
85. Wei P, Sun M, Yang B, Xiao J, Du J. Ultrasound-responsive polymersomes capable of endosomal escape for efficient cancer therapy. *J Control Release*. 2020; 322: 81-94.
86. Cheng DB, Zhang XH, Chen Y, Chen H, Qiao ZY, Wang H. Ultrasound-activated cascade effect for synergistic orthotopic pancreatic cancer therapy. *iScience*. 2020; 23: 101144.
87. Cheng CA, Chen W, Zhang L, Wu HH, Zink JI. Magnetic resonance imaging of high-intensity focused ultrasound-stimulated drug release from a self-reporting core@shell nanoparticle platform. *Chem Commun (Camb)*. 2020; 56: 10297-300.
88. Ding Z, Guo Z, Zheng Y, Wang Z, Fu Q, Liu Z. Radiotherapy reduces N-Oxides for prodrug activation in tumors. *J Am Chem Soc*. 2022; 144: 9458-64.
89. Shao D, Zhang F, Chen F, Zheng X, Hu H, Yang C, et al. Biomimetic diselenide-bridged mesoporous organosilica nanoparticles as an X-ray-responsive biodegradable carrier for chemo-immunotherapy. *Adv Mater*. 2020; 32: 2004385.
90. Guesdon-Vennerie A, Couvreur P, Ali F, Pouzoulet F, Roulin C, Martínez-Rovira I, et al. Breaking photoswitch activation depth limit using ionising radiation stimuli adapted to clinical application. *Nat Commun*. 2022; 13: 4102.
91. Hiruta Y. Poly(N-isopropylacrylamide)-based temperature- and pH-responsive polymer materials for application in biomedical fields. *Polym J*. 2022; 54: 1419-30.
92. Kolouchova K, Groborz O, Cernochova Z, Skarkova A, Brabek J, Rosel D, et al. Thermo- and ROS-responsive self-assembled polymer nanoparticle tracers for 19F MRI theranostics. *Biomacromolecules*. 2021; 22: 2325-37.
93. Li J, Pu K. Semiconducting polymer nanomaterials as near-infrared photoactivatable protherapeutics for cancer. *Acc Chem Res*. 2020; 53: 752-62.
94. Gong L, Zhang Y, Zhao J, Zhang Y, Tu K, Jiao L, et al. All-in-one biomimetic nanopatform based on hollow polydopamine nanoparticles for synergistically enhanced radiotherapy of colon cancer. *Small*. 2022; 18: 2107656.
95. Kano S, Takagi K, Yamaminami T, Takemura Y, Yusa S-i. pH-and thermoresponsive aggregation behavior of polymer-grafted magnetic nanoparticles. *Polym J*. 2021; 53: 1011-8.
96. Liu T, Li L, Wang S, Dong F, Zuo S, Song J, et al. Hybrid chalcogen bonds in prodrug nanoassemblies provides dual redox-responsivity in the tumor microenvironment. *Nat Commun*. 2022; 13: 7228.
97. Zhang P, Gao D, An K, Shen Q, Wang C, Zhang Y, et al. A programmable polymer library that enables the construction of stimuli-responsive nanocarriers containing logic gates. *Nat Chem*. 2020; 12: 381-90.
98. Fu C, Wei R, Xu P, Luo S, Zhang C, Kankala RK, et al. Supercritical fluid-assisted fabrication of diselenide-bridged polymeric composites for improved indocyanine green-guided photodynamic therapy. *Chem Eng J*. 2021; 407: 127108.
99. Lin H, Zhou Y, Wang J, Wang H, Yao T, Chen H, et al. Repurposing ICG enables MR/PA imaging signal amplification and iron depletion for iron-overload disorders. *Sci Adv*. 2021; 7: eabl5862.
100. Li H, Zeng Y, Zhang H, Gu Z, Gong Q, Luo K. Functional gadolinium-based nanoscale systems for cancer theranostics. *J Control Release*. 2021; 329: 482-512.
101. Yang R, Gao Y, Ouyang Z, Shi X, Shen M. Gold nanostar-based complexes applied for cancer theranostics. *View (Beijing)*. 2022; 3: 20200171.
102. Liu Y, Quan X, Li J, Huo J, Li X, Zhao Z, et al. Liposomes embedded with PEGylated iron oxide nanoparticles enable ferroptosis and combination therapy in cancer. *Natl Sci Rev*. 2023; 10: nwac167.
103. Barani M, Rahdar A, Mukhtar M, Razaq S, Qindeel M, Hosseini Olam SA, et al. Recent application of cobalt ferrite nanoparticles as a theranostic agent. *Mater Today Chem*. 2022; 26: 101131.
104. Hou J, Zhao Y, Sun L, Zou X. Enzyme/GSH/pH-responsive hyaluronic acid grafted porous silica nanocarriers bearing Ag(2)S QDs for fluorescence imaging and combined therapy. *Carbohydr Polym*. 2023; 305: 120547.
105. Liang Q, Chen J, Hou S, Li D, Zhu Y, Li R, et al. Activatable Mn(2+)-Armed nanoagonist augments antitumor immunity in colorectal cancer: a NIR-II Photonic neoadjuvant paradigm. *Biomaterials*. 2023; 300: 122206.
106. Lin X, Li W, Wen Y, Su L, Zhang X. Aggregation-induced emission (AIE)-based nanocomposites for intracellular biological process monitoring and photodynamic therapy. *Biomaterials*. 2022; 287: 121603.
107. Bodei L, Herrmann K, Schöder H, Scott AM, Lewis JS. Radiotheranostics in oncology: current challenges and emerging opportunities. *Nat Rev Clin Oncol*. 2022; 19: 534-50.
108. Zhang H, Zhao H, Huang Y, Sun G, Zhang Y. Microenvironment-activatable cascaded responsive carbonized polymer dots as a theranostic platform for precise rapamycin delivery to potentiate the synergy of chemotherapy and $\gamma\delta$ T cells-mediated immunotherapy against tumor. *Appl Mater Today*. 2022; 26: 101364.
109. Chen T, Su L, Ge X, Zhang W, Li Q, Zhang X, et al. Dual activated NIR-II fluorescence and photoacoustic imaging-guided cancer chemo-radiotherapy using hybrid plasmonic-fluorescent assemblies. *Nano Res*. 2020; 13: 3268-77.
110. Chen T, Zeng W, Tie C, Yu M, Hao H, Deng Y, et al. Engineered gold/black phosphorus nanopatforms with remodeling tumor microenvironment for sonoactivated catalytic tumor theranostics. *Bioact Mater*. 2022; 10: 515-25.
111. Sun S, Wang D, Yin R, Zhang P, Jiang R, Xiao C. A Two-in-one nanoprodrug for photoacoustic imaging-guided enhanced sonodynamic therapy. *Small*. 2022; 18: 2202558.
112. Wang F, Yu Q, Li J, Jiang J, Deng T, Yu C. Biomimetic macrophage membrane-coated gold-quantum dots with tumor microenvironment stimuli-responsive capability for tumor theranostic. *Mater Today Bio*. 2022; 16: 100359.
113. Wang C, Wang Q, Wang H, Li Z, Chen J, Zhang Z, et al. Hydroxyethyl starch-folic acid conjugates stabilized theranostic nanoparticles for cancer therapy. *J Control Release*. 2023; 353: 391-410.
114. Zhu C, Wang Y, Li Z, Sun W, Jiang BP, Shen XC. Metallopolysaccharide-based smart nanotheranostic for imaging-guided precise phototherapy and sequential enzyme-activated ferroptosis. *Biomacromolecules*. 2022; 23: 2007-18.
115. Zhou F, Yang S, Zhao C, Liu W, Yao X, Yu H, et al. γ -Glutamyl transpeptidase-activatable near-infrared nanoassembly for tumor fluorescence imaging-guided photothermal therapy. *Theranostics*. 2021; 11: 7045-56.
116. Pei Q, Lu S, Zhou J, Jiang B, Li C, Xie Z, et al. Intracellular enzyme-responsive profluorophore and prodrug nanoparticles for tumor-specific imaging and precise chemotherapy. *ACS Appl Mater Interfaces*. 2021; 13: 59708-19.
117. Hai X, Zhu X, Yu K, Yue S, Song W, Bi S. Dual-mode glucose nanosensor as an activatable theranostic platform for cancer cell recognition and cascades-enhanced synergetic therapy. *Biosens Bioelectron*. 2021; 192: 113544.
118. Yao S, Chen Y, Xu H, Qi F, Zhang Y, Yang T, et al. Hypoxia-responsive near infrared thioxanthene-hemicyanine nanoparticle for multimodal imaging-guided photothermal/photodynamic therapy. *Dyes Pigm*. 2022; 206: 110583.
119. Lai Y, Dang Y, Li F, Ding C, Yu H, Zhang W, et al. Reactive glycolysis metabolite-activatable nanotheranostics for NIR-II fluorescence imaging-guided phototherapy of cancer. *Adv Funct Mater*. 2022; 32: 2200016.

120. Jia X, Lv M, Fei Y, Dong Q, Wang H, Liu Q, et al. Facile one-step synthesis of NIR-responsive siRNA-Inorganic hybrid nanoplatform for imaging-guided photothermal and gene synergistic therapy. *Biomaterials*. 2022; 282: 121404.
121. Su L, Liu Y, Zhu Y, Guo F, Arkin G, Lin X, et al. Photo-responsive NIR-II biomimetic nanomedicine for efficient cancer-targeted theranostics. *Mater Today Chem*. 2022; 24: 100879.
122. Gao D, Shi Y, Ni J, Chen S, Wang Y, Zhao B, et al. NIR/MRI-guided oxygen-independent carrier-free anti-tumor nano-theranostics. *Small*. 2022; 18: 2106000.
123. Xu C, Huang J, Jiang Y, He S, Zhang C, Pu K. Nanoparticles with ultrasound-induced afterglow luminescence for tumour-specific theranostics. *Nat Biomed Eng*. 2023; 7: 298-312.
124. Seo Y, Ghazanfari L, Master A, Vishwasrao HM, Wan X, Sokolsky-Papkov M, et al. Poly(2-oxazoline)-magnetite NanoFerrogels: magnetic field responsive theranostic platform for cancer drug delivery and imaging. *Nanomedicine*. 2022; 39: 102459.
125. Choi PS, Lee JY, Chae JH, Wadas T, Cheng Z, Hur MG, et al. Theranostics through utilizing cherenkov radiation of radioisotope Zr-89 with a nanocomposite combination of TiO(2) and MnO(2). *ACS Appl Mater Interfaces*. 2023; 15: 3689-98.
126. Oroojalian F, Karimzadeh S, Javanbakht S, Hejazi M, Baradaran B, Webster TJ, et al. Current trends in stimuli-responsive nanotheranostics based on metal-organic frameworks for cancer therapy. *Mater Today (Kidlington)*. 2022; 57: 192-224.
127. She W, Pan D, Luo K, He B, Cheng G, Zhang C, et al. PEGylated dendrimer-doxorubicin conjugates as pH-sensitive drug delivery systems: synthesis and in vitro characterization. *J Biomed Nanotechnol*. 2015; 11: 964-78.
128. Li Z, Cai H, Li Z, Ren L, Ma X, Zhu H, et al. A tumor cell membrane-coated self-amplified nanosystem as a nanovaccine to boost the therapeutic effect of anti-PD-L1 antibody. *Bioact Mater*. 2023; 21: 299-312.
129. Zhu J, Xiao T, Zhang J, Che H, Shi Y, Shi X, et al. Surface-charge-switchable nanoclusters for magnetic resonance imaging-guided and glutathione depletion-enhanced photodynamic therapy. *ACS Nano*. 2020; 14: 11225-37.
130. Zhu X, Li L, Tang J, Yang C, Yu H, Liu K, et al. Cascade-responsive nano-assembly for efficient photothermal-chemo synergistic inhibition of tumor metastasis by targeting cancer stem cells. *Biomaterials*. 2022; 280: 121305.
131. Liu M, Huang L, Zhang W, Wang X, Geng Y, Zhang Y, et al. A transistor-like pH-sensitive nanodetergent for selective cancer therapy. *Nat Nanotechnol*. 2022; 17: 541-51.
132. van Hest J, Sun B, Guo X, Feng M, Cao S, Yang H, et al. Responsive peptide nanofibers with theranostic and prognostic capacity. *Angew Chem Int Ed Engl*. 2022; 61: 202208732.
133. Guan G, Zhang C, Liu H, Wang Y, Dong Z, Lu C, et al. Ternary alloy PtWmn as a Mn nanoreservoir for high-field MRI monitoring and highly selective ferroptosis therapy. *Angew Chem Int Ed Engl*. 2022; 61: 202117229.
134. Mao J, Li Y, Cai Q, Tang Z, Yang Y, Yuan C, et al. Tumor microenvironment-activated self-charge-generable metallosupramolecular polymer nanocapsules for photoacoustic imaging-guided targeted synergistic photothermal-chemotherapy. *Chem Eng J*. 2021; 405: 126690.
135. Yang RQ, Wang PY, Lou KL, Dang YY, Tian HN, Li Y, et al. Biodegradable nanoprobe for NIR-II fluorescence image-guided surgery and enhanced breast cancer radiotherapy efficacy. *Adv Sci (Weinh)*. 2022; 9: 2104728.
136. Lin W, Liu H, Chen L, Chen J, Zhang D, Cheng Q, et al. Pre-clinical MRI-guided intravesical instillation theranosis of bladder cancer by tumor-selective oxygen nanogenerator. *Nano Today*. 2021; 38: 101124.
137. Yang B, Zhang Y, Sun L, Wang J, Zhao Z, Huang Z, et al. Modulated ultrasmall γ -Fe₂O₃ nanocrystal assemblies for switchable magnetic resonance imaging and photothermal-ferroptotic-chemical synergistic cancer therapy. *Adv Funct Mater*. 2023; 33: 2211251.
138. Wang Q, Yu Y, Chang Y, Xu X, Wu M, Ediriweera GR, et al. Fluoropolymer-MOF hybrids with switchable hydrophilicity for (19)F MRI-monitored cancer therapy. *ACS Nano*. 2023; 17: 8483-98.
139. Lu C, Li Z, Wu N, Lu D, Zhang XB, Song G. Tumor microenvironment-tailored nanoplatform for companion diagnostic applications of precise cancer therapy. *Chem*, in press. doi: 10.1016/j.chempr.2023.06.011.
140. Luo L, Qi Y, Zhong H, Jiang S, Zhang H, Cai H, et al. GSH-sensitive polymeric prodrug: synthesis and loading with photosensitizers as nanoscale chemo-photodynamic anti-cancer nanomedicine. *Acta Pharm Sin B*. 2022; 12: 424-36.
141. Wang S, Zhang L, Zhao J, He M, Huang Y, Zhao S. A tumor microenvironment-induced absorption red-shifted polymer nanoparticle for simultaneously activated photoacoustic imaging and photothermal therapy. *Sci Adv*. 2021; 7: eabe3588.
142. Liu L, Zhang J, An R, Xue Q, Cheng X, Hu Y, et al. Smart nanosensitizers for activatable sono-photodynamic immunotherapy of tumors by redox-controlled disassembly. *Angew Chem Int Ed Engl*. 2023; 62: 202217055.
143. Ren Z, Sun S, Sun R, Cui G, Hong L, Rao B, et al. A metal-polyphenol-coordinated nanomedicine for synergistic cascade cancer chemotherapy and chemodynamic therapy. *Adv Mater*. 2020; 32: 1906024.
144. Brito B, Ruggiero MR, Price TW, da Costa Silva M, Genicio N, Wilson AJ, et al. Redox double-switch cancer theranostics through Pt(IV) functionalised manganese dioxide nanostructures. *Nanoscale*. 2023; 15: 10763-75.
145. Zeng Q, Li X, Xie S, Xing D, Zhang T. Specific disruption of glutathione-defense system with activatable single molecule-assembled nanoprodrug for boosted photodynamic/chemotherapy eradication of drug-resistant tumors. *Biomaterials*. 2022; 290: 121867.
146. Yu J, He X, Zhang Q, Zhou D, Wang Z, Huang Y. Iodine conjugated Pt(IV) nanoparticles for precise chemotherapy with Iodine-Pt guided computed tomography imaging and biotin-mediated tumor-targeting. *ACS Nano*. 2022; 16: 6835-46.
147. Yu K, Hai X, Yue S, Song W, Bi S. Glutathione-activated DNA-Au nanomachine as targeted drug delivery platform for imaging-guided combinational cancer therapy. *Chem Eng J*. 2021; 419: 129535.
148. Zhang L, Zhuang W, Yuan Y, Shen J, Shi W, Liu G, et al. Novel glutathione activated smart probe for photoacoustic imaging, photothermal therapy, and safe posturgery treatment. *ACS Appl Mater Interfaces*. 2022; 14: 24174-86.
149. Li CQ, Ma MW, Zhang B, Chen W, Yin ZY, Xie XT, et al. A self-assembled nanoplatform based on Ag(2)S quantum dots and tellurium nanorods for combined chemo-photothermal therapy guided by H(2)O(2)-activated near-infrared-II fluorescence imaging. *Acta Biomater*. 2022; 140: 547-60.
150. Mu X, Huang Z, Feng W, Zhai M, Wang Y, Zhou D, et al. Zwitterionic rhodamine-CPT prodrug nanoparticles with GSH/H(2)O(2) responsiveness for cancer theranostics. *Theranostics*. 2023; 13: 267-77.
151. Liu L, Liu F, Liu D, Yuan W, Zhang M, Wei P, et al. A smart theranostic prodrug system activated by reactive oxygen species for regional chemotherapy of metastatic cancer. *Angew Chem Int Ed Engl*. 2022; 61: 202116807.
152. Shi C, Zhang Q, Yao Y, Zeng F, Du C, Nijjati S, et al. Targeting the activity of T cells by membrane surface redox regulation for cancer theranostics. *Nat Nanotechnol*. 2023; 18: 86-97.
153. Qin W, Huang J, Yang C, Yue Q, Chen S, Wang M, et al. Protease-activatable nanozyme with photoacoustic and tumor-enhanced magnetic resonance imaging for photothermal ferroptosis cancer therapy. *Adv Funct Mater*. 2023; 33: 2209748.
154. Cai H, Xiang Y, Zeng Y, Li Z, Zheng X, Luo Q, et al. Cathepsin B-responsive and gadolinium-labeled branched glycopolymer-PTX conjugate-derived nanotheranostics for cancer treatment. *Acta Pharm Sin B*. 2021; 11: 544-59.
155. Tang L, Wang Z, Mu Q, Yu Z, Jacobson O, Li L, et al. Targeting neutrophils for enhanced cancer theranostics. *Adv Mater*. 2020; 32: 2002739.
156. Chen A, Lu H, Cao R, Zhu Y, Li Y, Ge R, et al. A novel MMP-responsive nanoplatform with transformable magnetic resonance property for quantitative tumor bioimaging and synergetic chemo-photothermal therapy. *Nano Today*. 2022; 45: 101524.
157. Huang RH, Nayeem N, He Y, Morales J, Graham D, Klajn R, et al. Self-complementary zwitterionic peptides direct nanoparticle assembly and enable enzymatic selection of endocytic pathways. *Adv Mater*. 2022; 34: 2104962.
158. Cai H, Dai X, Wang X, Tan P, Gu L, Luo Q, et al. A nanostrategy for efficient imaging-guided antitumor therapy through a stimuli-responsive branched polymeric prodrug. *Adv Sci (Weinh)*. 2020; 7: 1903243.
159. Duan Z, Luo Q, Dai X, Li X, Gu L, Zhu H, et al. Synergistic therapy of a naturally inspired glycopolymer-based biomimetic nanomedicine harnessing tumor genomic instability. *Adv Mater*. 2021; 33: 2104594.
160. Ma D, Zong Q, Du Y, Yu F, Xiao X, Sun R, et al. Sequential enzyme-activated macrotheranostic probe for selective tumor mitochondria targeting. *Acta Biomater*. 2021; 135: 628-37.
161. Yang DC, Wen LF, Du L, Luo CM, Lu ZY, Liu JY, et al. A hypoxia-activated prodrug conjugated with a BODIPY-based photothermal agent for imaging-guided chemo-photothermal combination therapy. *ACS Appl Mater Interfaces*. 2022; 14: 40546-58.
162. Zhu H, Li Q, Shi B, Ge F, Liu Y, Mao Z, et al. Dual-emissive platinum(II) metallacage with a sensitive oxygen response for imaging of hypoxia and imaging-guided chemotherapy. *Angew Chem Int Ed Engl*. 2020; 59: 20208-14.
163. Zhou R, Xu H, Qu J, Ohulchanskyy TY. Hemoglobin nanocrystals for drugs free, synergistic theranostics of colon tumor. *Small*. 2023; 19: 2205165.
164. Zhang Y, Fang J, Ye S, Zhao Y, Wang A, Mao Q, et al. A hydrogen sulphide-responsive and depleting nanoplatform for cancer photodynamic therapy. *Nat Commun*. 2022; 13: 1685.
165. Wu Y, Zeng M, Cheng Q, Huang C. Recent progress toward physical stimuli-responsive emulsions. *Macromol Rapid Commun*. 2022; 43: 2200193.
166. Fang Y, Cheng J, Shen Z, You T, Ding S, Hu J. Ultrasound-mediated release of gaseous signaling molecules for biomedical applications. *Macromol Rapid Commun*. 2022; 43: 2100814.
167. An J, Hong H, Won M, Rha H, Ding Q, Kang N, et al. Mechanical stimuli-driven cancer therapeutics. *Chem Soc Rev*. 2023; 52: 30-46.
168. Wang Y, Gong N, Ma C, Zhang Y, Tan H, Qing G, et al. An amphiphilic dendrimer as a light-activatable immunological adjuvant for in situ cancer vaccination. *Nat Commun*. 2021; 12: 4964.
169. Qi Y, Miyahara M, Iwata S, Miyako E. Light-activatable liquid metal immunostimulants for cancer nanotheranostics. *Adv Funct Mater*, in press. doi: 10.1002/adfm.202305886.
170. Xu Z, Huang H, Xiong X, Wei X, Guo X, Zhao J, et al. A near-infrared light-responsive extracellular vesicle as a "Trojan horse" for tumor deep penetration and imaging-guided therapy. *Biomaterials*. 2021; 269: 120647.
171. Yao X, Yang B, Li C, He Q, Yang W. Second near-infrared light-activatable CO nanogenerator for enhanced cancer photo-theranostics. *Chem Eng J*. 2023; 453: 139888.

172. Li J, Kang M, Zhang Z, Li X, Xu W, Wang D, et al. Synchronously manipulating absorption and extinction coefficient of semiconducting polymers via precise dual-acceptor engineering for NIR-II excited photothermal theranostics. *Angew Chem Int Ed Engl.* 2023; 62: 202301617.
173. Shi Z, Bai H, Wu J, Miao X, Gao J, Xu X, et al. Acceptor engineering produces ultrafast nonradiative decay in NIR-II Aza-BODIPY nanoparticles for efficient osteosarcoma photothermal therapy via concurrent apoptosis and pyroptosis. *Research (Wash D C).* 2023; 6: 0169.
174. Ni Z, Zhang D, Zhen S, Liang X, Gong X, Zhao Z, et al. NIR light-driven pure organic Janus-like nanoparticles for thermophoresis-enhanced photothermal therapy. *Biomaterials.* 2023; 301: 122261.
175. Zhang Z, Xia T, Ran P, Wei J, Meng J, Zhang G, et al. Persistent luminescence-activated Janus nanomotors with integration of photodynamic and photothermal cancer therapies. *Chem Eng J.* 2023; 457: 141226.
176. Li D, Yang Y, Li D, Pan J, Chu C, Liu G. Organic sonosensitizers for sonodynamic therapy: from small molecules and nanoparticles toward clinical development. *Small.* 2021; 17: 2101976.
177. Nguyen Cao TG, Kang JH, Kim W, Lim J, Kang SJ, You JY, et al. Engineered extracellular vesicle-based sonotheranostics for dual stimuli-sensitive drug release and photoacoustic imaging-guided chemo-sonodynamic cancer therapy. *Theranostics.* 2022; 12: 1247-66.
178. Huo S, Liao Z, Zhao P, Zhou Y, Göstl R, Herrmann A. Mechano-nanoswitches for ultrasound-controlled drug activation. *Adv Sci (Weinh).* 2022; 9: 2104696.
179. Liu T, Wan Q, Zou C, Chen M, Wan G, Liu X, et al. Stepwise drug release from a nanoplatform under MR-assisted focused ultrasound stimulation. *Chem Eng J.* 2021; 417: 128004.
180. Sabuncu S, Montoya Mira J, Quentel A, Gomes MM, Civitci F, Fischer JM, et al. Protein-coated biodegradable gas-stabilizing nanoparticles for cancer therapy and diagnosis using focused ultrasound. *Adv Mater Interfaces.* 2023; 10: 2201543.
181. Yu B, Choi B, Li W, Kim DH. Magnetic field boosted ferroptosis-like cell death and responsive MRI using hybrid vesicles for cancer immunotherapy. *Nat Commun.* 2020; 11: 3637.
182. Luo Q, Duan Z, Li X, Gu L, Ren L, Zhu H, et al. Branched polymer-based redox/enzyme-activatable photodynamic nanoagent to trigger STING-dependent immune responses for enhanced therapeutic effect. *Adv Funct Mater.* 2022; 32: 2110408.
183. Wang N, Zeng Q, Zhang R, Xing D, Zhang T. Eradication of solid tumors by chemodynamic theranostics with H₂O₂-catalyzed hydroxyl radical burst. *Theranostics.* 2021; 11: 2334-48.
184. Chen X, Gao H, Deng Y, Jin Q, Ji J, Ding D. Supramolecular aggregation-induced emission nanodots with programmed tumor microenvironment responsiveness for image-guided orthotopic pancreatic cancer therapy. *ACS Nano.* 2020; 14: 5121-34.
185. Fang W, Song B, Han L, Tao J, Li Y, Tang R, et al. Spatiotemporal theranostic nanoprobe dynamically monitor targeted tumor therapy. *Adv Funct Mater*, in press. doi: 10.1002/adfm.202306174.
186. Yue R, Zhou M, Li X, Xu L, Lu C, Dong Z, et al. GSH/APE1 cascade-activated nanoplatform for imaging therapy resistance dynamics and enzyme-mediated adaptive ferroptosis. *ACS Nano.* 2023; 17: 13792-810.
187. Wang M, Zhang X, Chang Q, Zhang H, Zhang Z, Li K, et al. Tumor microenvironment-mediated NIR-I-to-NIR-II transformation of Au self-assembly for theranostics. *Acta Biomater.* 2023; 168: 606-16.
188. Zeng F, Tang L, Zhang Q, Shi C, Huang Z, Nijati S, et al. Coordinating the mechanisms of action of ferroptosis and the photothermal effect for cancer theranostics. *Angew Chem Int Ed Engl.* 2022; 61: 202112925.
189. Wu J, Zhang Y, Jiang K, Wang X, Blum NT, Zhang J, et al. Enzyme-engineered conjugated polymer nanoplatform for activatable companion diagnostics and multistage augmented synergistic therapy. *Adv Mater.* 2022; 34: 2200062.
190. Gou S, Chen N, Wu X, Zu M, Yi S, Ying B, et al. Multi-responsive nanotheranostics with enhanced tumor penetration and oxygen self-producing capacities for multimodal synergistic cancer therapy. *Acta Pharm Sin B.* 2022; 12: 406-23.
191. Tang D, Yu Y, Zhang J, Dong X, Liu C, Xiao H. Self-sacrificially degradable pseudo-semiconducting polymer nanoparticles that integrate NIR-II fluorescence bioimaging, photodynamic immunotherapy, and photo-activated chemotherapy. *Adv Mater.* 2022; 34: 2203820.
192. Zhou C, Zhang L, Sun T, Zhang Y, Liu Y, Gong M, et al. Activatable NIR-II plasmonic nanotheranostics for efficient photoacoustic imaging and photothermal cancer therapy. *Adv Mater.* 2021; 33: 2006532.
193. Li W, Yin S, Shen Y, Li H, Yuan L, Zhang XB. Molecular engineering of pH-responsive NIR oxazine assemblies for evoking tumor ferroptosis via triggering lysosomal dysfunction. *J Am Chem Soc.* 2023; 145: 3736-47.
194. Chen Z, Sun Y, Wang J, Zhou X, Kong X, Meng J, et al. Dual-responsive triple-synergistic Fe-MOF for tumor theranostics. *ACS Nano.* 2023; 17: 9003-13.
195. Zhao M, Zeng Q, Li X, Xing D, Zhang T. Aza-BODIPY-based phototheranostic nanoagent for tissue oxygen auto-adaptive photodynamic/photothermal complementary therapy. *Nano Res.* 2022; 15: 716-27.
196. Sang X, Gao T, Liu X, Shen Y, Chang L, Fu S, et al. Two-wave variable nanotheranostic agents for dual-mode imaging-guided photo-induced triple-therapy for cancer. *Adv Sci (Weinh).* 2022; 9: 2201834.
197. Hu A, Pu Y, Xu N, Cai Z, Sun R, Fu S, et al. Controlled intracellular aggregation of magnetic particles improves permeation and retention for magnetic hyperthermia promotion and immune activation. *Theranostics.* 2023; 13: 1454-69.
198. Tan P, Chen X, Zhang H, Wei Q, Luo K. Artificial intelligence aids in development of nanomedicines for cancer management. *Semin Cancer Biol.* 2023; 89: 61-75.
199. Pan D, Zheng X, Zhang L, Li X, Zhu G, Gong M, et al. Synergistic disruption of metabolic homeostasis through hyperbranched poly(ethylene glycol) conjugates as nanotherapeutics to constrain cancer growth. *Adv Mater.* 2022; 34: 2109036.